Millennial-scale Iron Flux and Ocean Circulation Change Affects Subantarctic Pacific Carbon Cycling During Marine Isotope Stage 3 (57-29 ka)

H.J. Anderson[1], Z. Chase[1], H.C. Bostock[2,3], T.L. Noble[1], R. Shuttleworth[4], B. Taiapa[5], W.H. Chen[6], H. Ren[6], G.E. Jacobsen[7]

[1] Institute for Marine and Antarctic Studies, University of Tasmania, Hobart, Tasmania, Australia.

[2] School of Earth and Environmental Sciences, University of Queensland, Brisbane, Queensland, Australia.

[3] National Institute of Water and Atmospheric Research (NIWA), Wellington, New Zealand.

[4] School of Ocean and Earth Science, University of Southampton, National Oceanography Centre Southampton, Waterfront Campus, European Way, Southampton, United Kingdom

[5] Victoria University, Wellington, New Zealand

[6] Department of Geosciences, National Taiwan University, Taipei, Taiwan

[7] Center for Accelerator Science, Australian Nuclear Science and Technology Organisation, Lucas Heights, NSW, Australia

Corresponding Author: Harris Anderson, harris.anderson@utas.edu.au

Key points

1 – Decreased iron from New Zealand limits subantarctic Pacific export production during MIS-3 warming events.

2 –Increased nitrate supply to subantarctic waters may result from a southward shift of SWW and/or Southern Ocean fronts during MIS-3 warming events.

3 – Expansion of PDW and strengthened South Pacific convection may drive low bottom water oxygen at TAN1106-28 during MIS-3 warming events.

Abbreviations

MIS-3: Marine Isotope Stage 3

SO: Southern Ocean

FB- ^{15}N: Foraminiferal Bound FB- ^{15}N

AIM: Antarctic Isotope Maxima

AMOC: Atlantic Meridional Overturning Circulation

SWW: Southern Hemisphere Westerly Winds

EDC: EPICA Dome C Ice Core

Abstract

During Marine Isotope Stage 3 (MIS-3; 57–29 ka) Antarctic ice cores reveal a glacial climate state punctuated by millennial-scale warming events and pulses of CO_2. Changes in iron-fertilised export production and ocean circulation/upwelling, interpreted from South Atlantic sediment cores, suggest that the Southern Ocean is a conduit for the storage and release of CO_2 from the deep ocean. However, it is unclear whether this occurs throughout the Southern Ocean as these processes have not previously been investigated in the southwest Pacific . Here we describe localised iron limitation linked to glaciation changes in New Zealand, which reduced export production during early MIS-3 (60–48 ka) and caused decreases/increases in export production during late MIS-3 (48–29 ka) millennial-scale warming/cooling. Consistent decreases in foraminifera-bound ^{15}N during all MIS-3 warming events may reflect changes in the supply of nitrate to the subantarctic Pacific, possibly from increased wind-driven upwelling in the Antarctic and northward eddy-driven transport and/or shifting SO fronts. Concomitant decreases in bottom water oxygen and increases in the ^{14}C age of deep waters suggest that old, nutrient-rich waters influenced upper circumpolar deep water in the southwest Pacific during warming events. This signature may reflect an expansion of Pacific Deep Water into the Southern Ocean as Southern Ocean overturning strengthens. Iron-limitation of export production, the expansion of Pacific Deep water, and increased wind-driven upwelling would all work to contribute to increasing atmospheric CO_2 through reduced drawdown, and increased outgassing from the Pacific carbon reservoir during the millennial-scale warming events of MIS-3.

Plain Language Summary

Antarctic ice cores have provided evidence of repeated warming and cooling of the Southern Hemisphere that took place over hundreds to thousands of years between 57,000–29,000 years ago. During these warming events the Southern Ocean is thought to have played a role in the increasing concentration of CO_2 in the atmosphere. Here we use a sediment core from the Pacific Southern Ocean to determine how reduced iron input to the surface ocean impacted biological productivity during warming events, which decreased the level of CO_2 sequestration in the region. We and proxies for deep water oxygen concentration, surface nutrient compositions, and the age of deep waters to identify how ocean circulation in the Pacific Southern Ocean may have produced conditions favourable for CO_2 release from the ocean interior during periods of warming. Our findings support the theory that the Southern Ocean played an important role in past carbon cycle variability by sequestering carbon in deep ocean during cooling periods and releasing carbon during episodes of warming.

Introduction

During the last glacial period the Southern Ocean (SO) is thought to have played an important role in modulating the concentration of atmospheric CO_2 (Gottschalk et al., 2016; Sigman et al., 2010; Martínez-García et al., 2014). In Antarctic ice cores Marine Isotope Stage 3 (MIS-3; 57—29 ka) was characterised by Antarctic Isotope Maxima (AIM events) —millennial-scale warming and cooling of Antarctica by 1—3°C, which were accompanied by atmospheric CO_2 rises of 15—30 ppm (Ahn & Brook, 2008; Bereiter et al., 2012). These warming events and their associated CO_2 increases are largest during Heinrich events – longer duration warming events accompanied by discharges of icebergs from the Laurentide ice sheet into the North Atlantic – which are thought to result in a near complete collapse of Atlantic Meridional Overturning Circulation (AMOC; Bohm et al., 2015). It has been suggested that these millennial-scale fluctuations in atmospheric CO_2 involve the storage and release of carbon from the deep SO (Bauska et al., 2018; Gottschalk et al., 2016; Jaccard et al., 2016; Ziegler et al., 2013). Changes in the efficiency of the biological pump, the amount of upwelling, and air-sea gas exchange south of the Polar Front (PF) have all been considered as SO controls on atmospheric CO_2 variability during MIS-3 (Jaccard et al., 2016). Changes in the efficiency of the biological pump are thought to be affected by the amount of bioavailable iron delivered as mineral dust to the high nutrient, low chlorophyll SO (Anderson et al., 2014; Shoenfelt et al., 2018). Whereas air sea-gas exchange is more dependent on a combination of the location and intensity of the Southern Hemisphere westerly winds, upwelling strength, sea-ice cover, temperature and polar ocean stratification (Anderson et al., 2009; Gottschalk et al., 2016; Jaccard et al., 2016; Sigman et al., 2010).

The mechanisms involved in modulating deep ocean carbon storage and release in response to millennial-scale climate changes have been reconstructed in a small number of records in the subantarctic Atlantic (Anderson et al., 2014; Gottschalk et al., 2016; Martínez-Garcia et al., 2009; Martínez-García et al., 2014; Ziegler et al., 2013). These records provide a strong consensus that during southern hemisphere (SH) cold periods of the last glacial period the amount and bioavailability of iron delivered to the surface SO increased (Jaccard et al., 2013; Lamy et al., 2014; Martínez-Garcia et al., 2009, 2011; Shoenfelt et al., 2018). This higher iron flux is associated with increased export production in the subantarctic Indian Ocean (Thöle et al., 2019) and export production and nutrient utilisation in the subantarctic Atlantic (Anderson et al., 2014; Martínez-García et al., 2014). In contrast, during the warming phases of the last glacial period (AIM events), reduced iron delivery and export production, alongside increased exchange of CO_2 between the deep ocean and the atmosphere is proposed to contribute to millennial-scale increases in atmospheric CO_2 (Gottschalk et al., 2016; Jaccard et al., 2016). Decreased ^{14}C ventilation ages that coincide with increases in oxygenation of Circumpolar Deep Water (CDW) has been used to argue for increased ventilation of deep waters and outgassing during these

warming events (Jaccard et al., 2016; Gottschalk et al., 2016). The mechanisms proposed to be driving this increased outgassing are reductions in sea ice extent (Stephens & Keeling, 2000; Ziegler et al., 2013; Gottschalk et al., 2016) and increased westerly wind strength (Anderson et al., 2009; Toggweiler et al., 2006), which together are suggested to expose and upwell deep waters to the surface south Atlantic. In contrast to the South Atlantic, records of millennial-scale biological and physical changes in the South Pacific are sparse. There is only one study, at site MD97-2120 that describes thorium normalised export production increases during AIM warming events in a short section of early MIS-3, between 56.2 and 44.9 ka (Sachs & Anderson, 2005). Additionally, one record from the central South Pacific shows dust flux decreases during AIM events (Shoenfelt et al., 2018). As a result, the mechanisms that control biological and physical processes in this region and their influence on CO_2 flux are poorly constrained.

In this paper we provide new evidence for millennial scale changes in iron flux, surface water productivity and bottom water oxygen (BWO) in the subantarctic southwest Pacific and compare them with previous work in the subantarctic Atlantic and Indian Oceans. We present a highly resolved sediment core from the subantarctic zone south of New Zealand (TAN1106-28; 48°22'19.20" S; 165°39'32.40" E; 2798 m; Figure 1) that spans the last 70 ka, but this study focusses on MIS-3. We utilise three temperature proxies (Foraminiferal modern analogue transfer function, Mg/Ca, and Alkenone Uk'_{37}) to identify millennial scale warming and cooling events during MIS-3. These events are used to align to Antarctic Isotope Maxima (AIM) in the Antarctic ice cores and to develop a detailed age model in conjunction with radiocarbon dates (following the approach used in Anderson et al., 2021). We then combine and compare ^{230}-Th-normalised fluxes of biological material (excess Ba, total organic carbon, and chlorins) with fluxes of lithogenic material (^{232}Th and Fe) and foraminiferal bound nitrogen isotopic compositions (a proxy for surface nitrate supply and utilisation) to determine the effects of iron fertilisation on the biological pump during warming events. We compare these findings against Antarctic ice core evidence of MIS-3 climate changes at EPICA Dome C (EDC; Jouzel et al., 2007; Lambert et al., 2012). Lastly, we use two proxies of deep ocean redox conditions (excess Mn, and authigenic U) alongside benthic-planktic ^{14}C age offsets to assess changes in deep water oxygenation and ocean circulation.

Setting

Sediment core TAN1106-28 (Figure 1) is located in the Solander Trough south of New Zealand. Sediment in the Solander Trough is primarily terrigenous and hemipelagic and is delivered from the Southern Alps via the Southland Current and the Solander Channel (Carter & McCave, 2002). The TAN1106-28 site is just south of the Subtropical front (STF; (Bostock et al., 2015; Smith et al., 2013). The STF acts as a boundary between warm, saline and micronutrient-poor subtropical waters to the north and the cooler, fresher, and macronutrient (NO_3^- and PO_4^{3-}) rich waters of the Southern Ocean to the south (Figure 1;

Belkin & Gordon, 1996; Bostock et al., 2015; Orsi et al., 1995). During the last glacial maximum Southern Ocean fronts are thought to have shifted northward 3—5° bathing the site in subantarctic waters (Bostock et al., 2015), which should have increased surface nitrate concentrations and reduced SST (Marr et al., 2013) in surface waters over TAN1106-28. However, evidence from the South Pacific suggests that surface nitrate concentrations were reduced in the Antarctic zone due to decreased upwelling during the last glacial period (Robinson & Sigman, 2008). So it is unclear how surface nitrate concentrations have changed at this core site.

The core site at 2798 m water depth currently sits at the boundary between Upper Circumpolar Deep Water (UCDW) and Lower Circumpolar Deep Water (LCDW) (Carter et al., 2008; Figure 2). UCDW in the region south of New Zealand is characterised by high salinity (34.75 g/kg), low oxygen (190 — 200 µmol/kg), near saturation of calcite (Ω =1.02) and moderate-high nutrient concentrations (NO_3^- = 32 µmol/kg) (Bostock et al., 2011; Lauvset et al., 2020; Talley et al., 2013). To the northeast (between 24—34°S) UCDW is influenced by PDW, which is characterised by slightly lower salinity (34.65 g/kg), lower oxygen (100 — 150 µmol/kg), lower calcite saturation state (~1 to <1) and higher nutrient concentrations (NO_3^- = ~36 µmol/kg) relative to UCDW (Bostock et al., 2011; Lauvset et al., 2020; Talley et al., 2013). During the last glacial maximum and MIS-4, Nd isotopic evidence suggests increased PDW influence on Circumpolar Deep Water (CDW) south of the Chatham Rise (44—46°S) relative to the Holocene (McCave et al., 2008; Noble et al., 2013; Pahnke & Zahn, 2005; Ronge et al., 2015).

Materials and Methods

Sea Surface Temperatures (SST)

Three temperature proxies were analysed at TAN1106-28. First, 22 foraminiferal modern analogue temperatures (F-MAT) were determined using the method outlined in Hayward et al., (2012) at GeoMarine Research, Auckland, New Zealand. Second, 50 magnesium to calcium ratios (Mg/Ca) were measured by ICP-MS on *Globigerina bulloides* following the methods in Shuttleworth et al., (2021) at the University of Southampton, United Kingdom, and converted to paleo-temperatures using the Elderfield and Ganssen (2000) calibration. Last, alkenone measurements were made on 44 samples (methods in Shuttleworth et al., 2021) at the University of Southampton, United Kingdom, and Alkenone unsaturation ratios ($U^{k'}_{37}$) were converted to paleo-temperature using the Sikes and Sicre (2002) calibration.

Each of these records was binned to 500-yr intervals, before calculating the mean temperature at each timestep to create a multi-proxy SST mean (Figure S1). This method both increases the resolution of the temperature reconstruction and reduces the uncertainty of the temperature record at the site (Anderson et al., 2021). Temperature uncertainty is represented by the standard error of the

mean, which is the root mean square error of the binned data at each time step (mean = ± 0.24°C), and by the mean proxy uncertainty (± 1.02°C), which is conservatively estimated as the mean of the three proxy uncertainties, which are ± 0.5 °C ($U^{k'}_{37}$), ± 0.88 °C (Mg/Ca), and ± 1.68°C (F-MAT).

^{14}C Analysis

The TAN1106-28 chronology was created with *Undatable* (Lougheed & Obrochta, 2019) using 19 mixed planktic foraminiferal^{14}C measurements and 8 tie points between the TAN1106-28 multi-proxy mean SST and the EPICA Dome C (EDC) D record on the AICC2012 timescale (Table 1; Figure 3; Jouzel et al., 2007; Veres et al., 2013) following the Anderson et al., (2021) method. We combined three previously published planktic ^{14}C dates (Bostock et al., 2015) and 16 new planktic ^{14}C dates (Table 1) analysed at the Australian Nuclear Science and Technology Organisation (ANSTO, Australia; n = 14), and at the Alfred Wegener Institute Germany; (n = 2). Radiocarbon was analysed on >2 mg mixed planktic foraminifera in the samples (avoiding deep dwelling planktic species) and nine mixed benthic foraminifera samples (> 2 mg) which were picked from depths that occurred closest to AIM event timings and had a paired planktic radiocarbon sample. The Benthic–Planktic radiocarbon age offset was determined by the difference between the mean calibrated ages of the benthic and planktic at the same depth. Radiocarbon measurements were calibrated using the MARINE20 radiocarbon calibration (Heaton et al., 2020), with a varying reservoir age (R) of 400 ± 100 years between 0—15 ka and a R of 1000 ± 200 years between 15 — 45 ka (Table 1; Butzin et al., 2017). TAN116028 R is calculated as the Butzin et al, (2017) minus the MARINE20 in-built reservoir age (Table 1). Age model uncertainty, which is a function of the density of age markers, ranges between 1000 — 2000 years during the Holocene and 750 — 1650 years during the last glacial period.

Elemental Concentrations and Compositions

Concentrations of Ba, Ca, Fe, Mn, ^{232}Th, ^{238}U and ^{230}Th in TAN1106-28 sediment samples were measured following a modified version of methods outlined in Durand et al., (2016; 2017), replacing the microwave step with hotplate digestion. Samples were analysed on a ThermoFischer Element 2 sector field ICP-MS at the University of Tasmania, with Ba, Ca, Fe, Mn, ^{232}Th and ^{238}U being analysed relative to external standards and ^{230}Th being measured by isotopic dilution. Repeat analysis of TAN1106-28: 0–1 cm and an in-house sediment standard (Chile Margin multi-core RR9702-42MC8) reveals standard deviations for Ba (3.2% and 6.2% respectively), Ca (4% and 3%), Fe (5.4% and 6%), Mn (5.3 % and 3.3%) and ^{238}U (1.5% and 4.8%) and less than 10% and 7% for ^{232}Th and less than 5% and 8% for ^{230}Th respectively.

Organic Carbon and Chlorin Concentrations

Total organic carbon concentration (TOC) was measured on 70 bulk sediment samples following a modified version of the method outlined in Hedges & Stern (1984). Sediment samples were sequentially acidified with 1M HCl (2 x 500 µL and 1x 300 µL) to remove carbonate (10—35%). Twenty milligram samples of this sediment were analysed on a ThermoFischer Elemental Analyser coupled to an Isotopic Ratio Mass Spectrometer at the University of Tasmania. To calculate TOC, the presence of additional Cl^- ions as $CaCl_2$ was corrected by 46.085 mg of additional Cl from HCl. A replicate sediment sample (n = 5) was analysed to assess reproducibility and gives a relative standard deviation of 10.12%.

Chlorins are degradation products of chlorophyll that are preserved in marine sediments (Harris & Maxwell 1995). Chlorin concentrations were measured using the progressive acetone leaching method of Higginson et al., (2003). Leachates were analysed using a Turner benchtop spectrophotometer and concentrations were compared to a chlorophyll calibration curve. A sediment sample was analysed in triplicate to assess reproducibility and gives a relative standard deviation of 1.04%.

Thorium Normalisation, Lithogenic Concentrations, and Excess ($_{xs}$) Metals

Calculations

The flux of lithogenic and biological material to the seafloor was calculated by normalising the respective concentrations of ^{232}Th and Fe, and Ba, TOC, chlorins, $CaCO_3$ to the concentration of ^{230}Th (Francois et al., 2004). Total ^{230}Th measurements were corrected for ingrowth of ^{230}Th from the decay of lithogenic and authigenic U assuming a detrital $^{238}U/^{232}Th$ activity of 0.7 ± 0.1 for the Pacific Ocean (Henderson & Anderson 2003). Concentrations of excess (subscript xs) Ba, Ca and Mn were calculated following the method in Chase et al., (2003), where the average continental crust ratio of a given trace metal to ^{232}Th (Rudnick & Gao, 2003) is subtracted from the total metal concentration and multiplied by the total ^{232}Th. The lithogenic component of sediments is estimated from ^{232}Th concentrations; we use an average continental value of 10 ppm assuming that ^{232}Th in samples is exclusively of detrital origin (Kienast et al., 2016; Rudnick & Gao, 2003).

Calcium Carbonate Concentrations

Calcium carbonate concentrations measured using the Jones & Kaiteris (1983) vacuum gasometic method, and are reported forTAN1106-28 in Bostock et al (2015). We have estimated $\%CaCO_3$ for the samples with ^{230}Th measurements using the $_{xs}$Ca concentration. This approach assumes that all $_{xs}$Ca originates from $CaCO_3$ in the sediments. This process reduces error associated with interpolating between sample depths to calculate $CaCO_3$ fluxes. $CaCO_3$ calculated

from $_{xs}$Ca was converted to a percentage and compares well (r^2 = 0.92, p = < 0.01) to discrete $CaCO_3$ measurements at TAN1106-28 from Bostock et al., (2015) (Figure S2).

Planktic Foraminiferal Bound ^{15}N

A minimum of 5 mg of planktonic foraminifera *Globigerina bulloides* were picked from 88 sample depths for foraminiferal bound nitrogen isotopic measurements. These samples were analysed using 'persulfate-denitrifier' method on a modified Sigbench and Thermo IRMS MAT 253 Plus at the National Taiwan University in Taipei following the method outlined in Ren et al., (2017). Analytical error for the whole procedure is less than 0.25‰.

Results

During MIS-3 AIM-warming events we observe a mean SST increase of 1.98 ± 0.6°C (Figure 5, AIM-warming events are highlighted in blue). Warming events are measured from the SST minimum that immediately precedes a warming event to the peak warming achieved during an AIM-warming event. These warming events coincide with warming events at EPICA Dome C, and the amplitude of these events is strongly correlated with the amplitude of warming at EDC (r^2 = 0.71, p < 0.01; Figure S2; Anderson et al., 2022).

The flux of iron and lithogenic material is strongly correlated during MIS-3 (Figure 4; r^2 = 0.83 p = < 0.01). During late MIS-3 (48–29 ka) AIM warming events we observe mean decreases in lithogenic flux of 2.26 ± 1.24 g cm^{-2} ka^{-1}, and iron flux of 0.21 ± 0.095 g cm^{-2} ka^{-1} (Figure 5). While there is a strong over all correlation, both lithogenic material flux and iron flux show considerably smaller changes during early MIS-3 AIM warming events (60–48 ka; Figure 5) iron flux shows little variation, with a small increase in each proxy occurring during the combined AIM cooling phases of AIM-17, AIM-16 and AIM-15 (59.5–57 ka).

Export production proxies; $_{xs}$Ba, chlorins, and TOC show a consistently well correlated pattern across MIS-3 (r^2 = 0.57 ($_{xs}$Ba/Chlorins), 0.62 ($_{xs}$Ba/TOC), 0.79 (TOC/Chlorins), p = < 0.01). During late MIS-3 warming events estimates of export production show decreases of 0.03 ± 0.02 g cm^{-2} ka^{-1} for TOC, 0.02 ± 0.005 g cm^{-2} ka^{-1} for $_{xs}$Ba, and 8.66e-5 ± 4.56e-5 g cm^{-2} ka^{-1} for chlorins (Figure 5). All three export production proxies are strongly correlated with the flux of iron (r^2 = 0.7 — 0.84, p= < 0.01; Figure 4.). However, $_{xs}$Ba is weakly correlated with lithogenic material flux (r^2 = 0.37, p = < 0.01), while chlorins and TOC are strongly correlated with lithogenic flux at TAN1106-28 (r^2 = 0.7 — 0.85, p = < 0.01). During early MIS-3 export production proxies exhibit a similar patter to iron flux, with little variation except a short-lived increase during the 56 ka stadial event. Conversely, carbonate flux is inversely correlated with the other export proxies and mean increases in $CaCO_3$ flux of 0.9 ± 0.31 g cm^{-2} ka^{-1} co-occur with SST rise (Figure 6).

We observe consistent decreases in FB- ^{15}N during AIM warming events (mean = 1.0 ± 0.5 ‰; Figure 5), which coincide with decreases in export production and iron flux during late MIS-3 (48—27 ka). Although, during the AIM warming events of early MIS-3, when there is little change in iron flux and export production, FB- ^{15}N decreases are of a magnitude that is consistent with those of late MIS-3 (Figure 5; Figure 6).

Millennial-scale decreases in BWO concentration are inferred from mean decreases in $_{xs}Mn$ of 151.04 ± 44 ppm and increases in authigenic uranium concentrations of 0.84 ± 0.09 dpm/g during AIM-warming events (Figure 7). Decreases in BWO coincide with surface warming and increased benthic-planktic ^{14}C age offsets (Figure 7).

Discussion

Millennial Scale Export Production Driven By Iron Fertilisation

Subantarctic Pacific SST increased by 0.5–4°C during the millennial-scale climate events of MIS-3 (Figure 5). The TAN1106-28 warming events are a similar magnitude to and coeval with SST increases across the subantarctic SO (Anderson et al., 2021), and Antarctic temperature increases at EPICA Dome C (Jouzel et al., 2007). We suggest that SST increases at TAN1106-28 occur as part of the thermal seesaw hypothesis, whereby AMOC slowdowns allow for an accumulation of heat in the SO (Pedro et al., 2018). In fact, we find that rates of warming at TAN1106-28 and Antarctica (EPICA Community Members, 2006) are not significantly different ($p = 0.15$), supporting the idea that the Antarctic climate and SO SST are similarly affected by AMOC slowdowns during MIS-3.

In the subantarctic Atlantic and Indian sectors of the SO these millennial-scale SST increases are associated with decreases in both lithogenic material flux and export production (Anderson et al., 2014; Gottschalk et al., 2016; Jaccard et al., 2016; Martínez-García et al., 2014; Thöle et al., 2019). In contrast, at TAN1106-28 we observe two distinct periods of MIS-3; early MIS-3, where lithogenic flux, iron flux, and export production are low despite varying SST, and late MIS-3, where increases in SST correspond with decreases in lithogenic flux, iron flux, and export production (Figure 6). However, increases in $CaCO_3$ flux are observed during all warming events (Figure 6), which warrant further examination (discussed later).

In the modern subantarctic Pacific biological productivity is demonstrably iron-limited (Peloquin et al., 2011; Leblanc et al., 2005; Hutchins et al., 2001). An iron addition experiment south of New Zealand in Subantarctic waters found a two-fold increase in primary production over the experiment duration (15 days), primarily stimulating the growth of picophytoplankton (Peloquin et al., 2011). Indeed, addition of iron and silicic acid in shipboard bottle incubation experiments show that the southwest Pacific and Australian subantarctic are demonstrably iron limited (Hutchins et al., 2001; Leblanc et al., 2005). Considering these experiments, iron fertilisation of biological productivity seems to be

an obvious interpretation of the strong positive correlation between export production ($_{xs}$Ba, TOC, Chlorins) and iron flux proxies (r^2 = 0.7–0.84; Figure 4) at TAN1106-28. However, the flux of lithogenic material and iron at TAN1106-28 is perennially high during MIS-3, being nearly twice as high as the nearby core MD97-2120 (Sachs & Anderson 2005), and nearly 20 times as high as the distal South Pacific core PS75/056-1 (Shoenfelt et al., 2018). Additionally, the TAN1106-28 lithogenic fluxes are also higher than at sites in the South Atlantic, and Indian sectors of the SO where aeolian deposition dominates the lithogenic supply (Anderson et al., 2014; Shoenfelt et al., 2018; Thöle et al., 2019).The high iron and lithogenic fluxes at TAN1106-28 result from the delivery of sediment associated with the uplift and erosion of New Zealand's Southern Alps and deep transport into the Solander trough (Carter & McCave, 2002). Indeed, Strontium and Neodymium isotopic results identify New Zealand as the primary source of lithogenic material (Trudgill et al., 2020). Additionally, the Westland and Southland Currents (Chiswell et al., 2015) may have increased fluvial transport of lithogenic sediment to the site during the glacial (Trudgill et al., 2020). Despite high total iron fluxes today, productivity at this site appears to be iron limited (see evidence presented in 'Setting' above). It may be that only a very small fraction of the total iron delivery to this region is bioavailable in surface waters.

Our results show that despite the high lithogenic fluxes at this site, iron availability likely determined the strength of the biological carbon pump during MIS-3 (Figure 5). During early MIS-3, we find that iron fluxes are at their lowest (60–48 ka; Figure 5). However, iron flux and export production then increases during the stadial periods of middle to late MIS-3 (48–29 ka). We suspect that export production may have responded to the supply of bioavailable iron, delivered in proportion to, but in lower concentrations than total iron/lithogenic flux. We propose that the low lithogenic and iron flux at TAN1106-28 during early MIS-3 is due to reduced glaciation with moraine deposit evidence for glacial retreat (Shulmeister et al., 2018; 2019), which is supported by the high SST during this time (60–48 ka = 10.7°C; Figure 5), and is compatible with low early MIS-3 iron flux in the subantarctic Atlantic (Martínez-García et al., 2014). This is consistent with the suggestion that glacial erosion markedly increases the bioavailability of transportable iron delivered to the SO (Shoenfelt et al., 2018), and with the inference that glaciation increased during later MIS-3 due to a northward shift in the Southern Hemisphere westerly winds (SWW; Shulmeister et al., 2019).

Variations in FB- ^{15}N provide support for iron fertilisation during late MIS-3 (48–29 ka; Figure 5). During this late MIS-3 period, we observe decreases in FB-^{15}N during AIM warming events that coincide with decreases in iron flux and export production, similar to what has been described in other regions of the subantarctic SO (Robinson et al., 2005; Martínez-García et al., 2014). However, during early MIS-3 (60–48 ka) AIM warming events, reductions in FB- ^{15}N of a similar amplitude to those of late MIS-3 occur without the corresponding decrease in export production (Figure 5). This suggests that it is variable nitrate

supply rather than iron-induced changes in nitrate utilisation that drives FB- ^{15}N variability during early MIS-3, and potentially also during late MIS-3.

Nitrate isotopic compositions in subantarctic surface waters reflect the combined effects of nutrient supply and nutrient utilisation. At TAN1106-28 we find consistent decreases in FB- ^{15}N during periods of increasing SST, and broadly decreasing iron flux and export production. However, during several MIS-3 AIM warming events, FB- ^{15}N decreases while export productivity and iron flux continues to increase, and FB- ^{15}N starts to rise when export production and iron flux remain low (Figure 5). This suggests that nutrient supply may be changing despite ongoing utilisation. Two processes may work to decouple changes in the ^{15}N from changes in the export production in this region. First, lateral transport of Antarctic surface nitrate to the Subantarctic could vary primarily due to changes in the strength of SWW and thus the intensity of the upwelling in the Antarctic. In the glacial period, Antarctic surface NO_3 concentrations are thought to be reduced relative to the present, likely due to reduced upwelling and increased water column stratification (Robinson & Sigman 2008). Across the last deglaciation and AIM warming events, increases in SSW strength are thought to drive upwelling (Anderson et al., 2009), which enhances the vertical supplies of nutrients to the Antarctic surface (Chiang et al., 2014; Toggweiler et al., 2006). Increases in SWW strength are also thought to stimulate eddy formation and northward Ekman advection of upwelled nutrients during the deglaciation and AIM warming events (Anderson et al., 2009; Chiang et al., 2014; Pedro et al., 2016). Thus, an increase in SWW strength during AIM warming events may have increased the advective supply of NO_3 to the TAN1106-28 site. However, a caveat to this interpretation is that the ^{15}N of the advected Antarctic surface nitrate is elevated compared to that of the subantarctic thermocline, due to partial nitrate assimilation by phytoplankton. As a result, an increase in lateral transport of Antarctic surface nitrate to the subantarctic during MIS-3 warming events may cause an initial increase in the ^{15}N, as seen in coral-based ^{15}N records from the Tasmanian subantarctic during the last deglaciation (Wang et al., 2017). However, our record at TAN1106-28 shows consistent decreases in the FB- ^{15}N across all the AIM warming events during MIS 3, suggesting that changes in the lateral transport of Antarctic surface nitrate alone cannot explain the decoupling between FB- ^{15}N and export productivity.

Secondly, as the subantarctic conditions change from high productivity, low surface nitrate ^{15}N at the subantarctic front, to low productivity, high surface nitrate ^{15}N at the subtropical, frontal migration associated with AIM warming events could work to decouple export production and ^{15}N at our core site. We expect that the SO fronts move southward when the SO surface warms (Pedro et al., 2016), which would feasibly bring the subtropical front closer to the modern day position near our core site. This could work to increase ^{15}N and while lowering the export productivity at our core site. In support for this mechanism, we note that during or immediately following several of the warm intervals (Figure 5), ^{15}N begins to rise while the export productivity stays low

for 1-2 kyr. While we cannot definitively exclude a variable effect from both increased lateral advection and a shift of the SO fronts, we do suggest that the overall changes in the FB- ^{15}N are consistent with iron fertilisation enhancement of export production, surface nutrient uptake, and SO carbon sequestration during MIS-3 AIM cooling phases (Anderson et al., 2014; Gottschalk et al., 2016; Martínez-García et al., 2014). In support for this argument, we find that there is a striking similarity between the timing and amplitude of microfossil-bound ^{15}N changes across the subantarctic Atlantic and open Pacific and at TAN1106-28 during MIS-3 AIM warming events (Figure S3; 1.0 ± 0.5 ‰ at TAN1106-28; 0.86 ± 0.42 ‰ at E11-2, Robinson et al., 2005; and 0.72 ± 0.41 ‰ at ODP-1090, Martínez-García et al., 2014).

Deep Ocean Dynamics and Circulation

During the majority of MIS-3 AIM warming events are associated with reduced BWO as indicated by increased authigenic uranium and decreased $_{xs}Mn$ at TAN1106-28 (Figure 7). These findings are in contrast to the increase in Atlantic CDW BWO during AIM warming events inferred from two sediment records between 3600–3800m (Gottschalk et al., 2016; Jaccard et al., 2016). At TAN1106-28 low BWO during AIM warming events is not due to increased respiration of organic carbon, as these periods are associated with reduced export production (Figure 6).

Decreasing BWO and increasing benthic-planktic ^{14}C age offsets at TAN1106-28 (Figure 7) are indicative of an old, low oxygen water mass bathing the southwest Pacific during AIM warming events. We consider two possible origins of this signal during AIM warming events in Pacific UCDW. Firstly, we consider a vertical shift in the LCDW/UCDW boundary as TAN1106-28 sits close to this boundary (Figure 2). At present LCDW is made up of modified NADW, and high oxygen Antarctic Bottom Water (AABW) that flows northward in the Pacific at depths greater than 3500 m (Kawano et al., 2006). If similar conditions existed during the last glacial period, then a reduced influence of LCDW would result in decreased oxygen in lower UCDW. Numerical modelling suggests that the isopycnal boundary between the upper and lower branches of the SO overturning cell shoaled by approximately 500 m during the last glacial period (Ferrari et al., 2014; Burke et al., 2015). Isopycnal shoaling would effectively bathe TAN1106-28 in high oxygen upper-LCDW during stadial periods, whereas during AIM warming events, a deepening of this boundary would bathe the site in lower oxygen PDW-influenced UCDW.

Secondly, we consider the possibility that decreasing BWO arises from PDW expansion, as these waters function as a source of UCDW in the Pacific (Talley 2013). During the last glacial period sediment core Mn concentration and $^{231}Pa/^{230}Th$ ratio records have been interpreted as the result of expansion of PDW into the Pacific sector of the SO, followed by increased ventilation of the abyssal Pacific during Heinrich Stadial 1 by oxygenated AABW (Pavia et al., 2021; Ronge et al., 2021). Ronge et al., (2021) suggests that these changes are

indicative of strengthening South Pacific overturning (greater AABW production) during the AMOC slowdown of Heinrich Stadial 1 (AIM-1), which also lead to an increase in transport of PDW to the South Pacific. In the previous section we inferred that FB- ^{15}N decreases during AIM warming events occurred due to a southward shift and intensification of the SWW (Chiang et al., 2014; Toggweiler et al., 2006), which shifts the centre of upwelling southward and increases its upwelling strength (Anderson et al., 2009). Anderson et al., (2009) suggests that a combination of Ekman-driven upwelling and buoyancy gain due to increased heat flux drove this upwelling. Numerical modelling suggest that increased AABW formation and decreased NADW influence during AIM warming events may have also driven increases in PDW formation in the North Pacific (Menviel et al., 2014), and may have created conditions that would bring low oxygen PDW to TAN1106-28. Numerical modelling also supports increases in SO overturning circulation that ventilates the deep SO (Skinner et al., 2020), and contributes to surface warming during AIM warming events (Pedro et al., 2016). Our results support the expanded PDW theory, as concomitant decreases in FB- ^{15}N and increases in both SST and deep water ^{14}C age during AIM events support increased SWW-driven upwelling, and a likely strengthening of South Pacific overturning circulation delivering PDW to the Subantarctic Pacific.

While we cannot definitively exclude either isopycnal shoaling, or expansion of PDW as drivers of BWO, we argue that neither process is mutually exclusive, and both are compatible with the pattern of BWO and benthic-planktic ^{14}C variability observed at TAN1106-28 (Figure 8). Additionally, we can reconcile southward expansion of PDW as part of strengthened South Pacific overturning circulation with bottom water ventilation in the South Atlantic during AIM warming events (Gottschalk et al., 2016; Jaccard et al., 2016). While the two basins exhibit differing BWO signals, we argue that they may track different limbs of the global/SO overturning circulation, with TAN1106-28 tracking the upper limb (UCDW), and the Atlantic sediment core records tracking the lower limb (LCDW/AABW; Ferrari et al., 2014).

Calcium Carbonate Flux and the Carbonate Counter Pump

Despite reduced iron flux during AIM warming events, we find increases in the flux of $CaCO_3$ that are at odds with the other paleo-productivity proxies and FB- ^{15}N. They are also difficult to reconcile with decreasing BWO during AIM warming events (Figure 6). Low BWO indicates that the export production decreases seen in TOC, $_{xs}Ba$, and Chlorins are not caused by increased respiration of organic matter. However, low oxygen conditions are typically associated with decreased carbonate saturation state, and therefore a decrease in carbonate preservation. This suggests the increases in $CaCO_3$ flux were instead driven by changes in carbonate production rather than by changes in carbonate preservation.

We suggest that $CaCO_3$ flux increases during AIM warming events were in response to SST, which increases coccolithophore production (Buitenhuis et al., 2008). Core TAN1106-28 sits south of the last glacial subtropical front, which is

associated with a 10°C isotherm in this region (Bostock et al., 2015). A southward migration of the STF near to TAN1106-28 during AIM warming events may drive increases in coccolithophore production (Duncan et al., 2016). In culture experiments, increasing temperature has also been shown to increase the ratio of $CaCO_3$ to organic biomass in coccolithophores — the ratio of particulate inorganic carbon (PIC) to particulate organic carbon (POC) (Krumhardt et al., 2017). Increases in the PIC:POC ratio have been suggested to improve preservation of $CaCO_3$ (Carter et al., 2000; Howard & Prell, 1994). Additionally, Increases in $CaCO_3$ production that occur during AIM warming events likely play an important role in the carbon cycle through the carbonate counter-pump. During periods of elevated $CaCO_3$ production a surface–depth alkalinity gradient is created which stimulates the release of CO_2 from the ocean to the atmosphere (Duchamp-Alphonse et al., 2018; Salter et al., 2014). The carbonate counter-pump should thus work to compound the effects of upwelling and reduced export production on atmospheric CO_2 concentrations from the southwest Pacific. Indeed, increases in coccolithophore production are observed at MD97-2120 as increases in $CaCO_3$ and alkenone flux during AIM-14 and AIM-12 (Sachs & Anderson 2005). As such, we suggest that during AIM warming events increases in SST and decreases in export production (TOC, $_{xs}$Ba, and chlorins) may result in an increase in $CaCO_3$ production and contribute to an increase in atmospheric CO_2.

We argue that decreases in iron-fertilised export production during late MIS-3 AIM-warming events that coincide with atmospheric CO_2 increase reflect a decrease in the efficiency of the subantarctic Pacific biological pump. Whereas, during early MIS-3 consistent low export production may support an extended period of reduced biological pump efficiency (Figure 5; Bereiter et al., 2015). We suggest that decreasing BWO and FB- ^{15}N during all MIS-3 AIM- warming events, supports a contribution of increased upwelling and outgassing of deep-stored CO_2 from the PDW in the Pacific SO regardless of export production change (Figure 7; Figure 8; Ahn & Brook, 2008; Bereiter et al., 2015).

Conclusions

In summary, our results support a contribution of subantarctic Pacific biological and physical processes to increases in atmospheric CO_2 during the millennial-scale climate changes of MIS-3. During periods of increased SST at TAN1106-28 reduced glaciogenic iron input results in decreased in export production and nutrient utilisation. The exception is during early MIS-3 (60–48 ka) when both iron flux and export production are reduced, likely due to warmer climate conditions and reduced glaciation in New Zealand. Increased SST and decreased Antarctic dust flux during AIM warming events may be indicative of a southward shift and intensification of the SWW, which we argue is supported by coincident decreases in FB- ^{15}N during AIM events. We suggest that FB- ^{15}N changes are primarily driven by variable nitrate supply during MIS-3, but broadly support decreases in nitrate utilisation during late MIS-3. AIM warming event decreases

in iron fertilisation of export production in the south Atlantic and at TAN1106-28 coincide with increases in atmospheric CO_2, strengthening the theory that a less efficient subantarctic biological pump plays a significant role in the global carbon cycle during MIS-3. Increased Southern Ocean overturning circulation during AIM warming events is inferred from a coincidence of surface warming, increased supply of nitrate, increased deep water ^{14}C age, and decreased BWO. We cannot definitively rule out the possibility that decreased BWO during AIM warming events may track a combination of both a decrease in the influence of LCDW due to a deepening isopycnal boundary between UCDW and LCDW, and an expansion of PDW into the SO during AIM warming events. However, the coincidence of increased deep water ^{14}C age and decreasing BWO points to an expansion of old CO_2 rich PDW expanding into the SO, which we suggest contributed to millennial-scale CO_2 pulses via air-sea gas exchange.

Open Research

Research data from sediment core TAN1106-28 is available on the PANGAEA database (DOI: Pending). This data includes age model data, paleo-reconstructions of SST, 230-Th normalised lithogenic material and iron fluxes, export production proxies, foraminiferal bound ^{15}N, authigenic uranium and excess manganese concentrations, and benthic-planktic ^{14}C age offsets.

Declaration of competing interest

The authors declare that they have no known competing financial interests or personal relationships that could have appeared to influence the work reported in this paper

Acknowledgments

We would like to thank the Captain Doug Monks and the crew of the RV Tangaroa on voyage TAN1106 on which the core was collected, funded by the National Institute of Water and Atmospheric Research core voyage funding. The redox, U/Th and $d^{15}N$ core analyses and Scholarship for HJA were funded by the Australian Research Council Discovery Project DP180102357 awarded to ZC and HB. This project received grant funding from the Australian Government as part of the Antarctic Science Collaboration Initiative program. The Australian Antarctic Program Partnership is led by the University of Tasmania, and includes the Australian Antarctic Division, CSIRO Oceans and Atmosphere, Geoscience Australia, the Bureau of Meteorology, the Tasmanian State Government and Australia's Integrated Marine Observing System. Funding for radiocarbon analyses at ANSTO was provided by an Australian Institute for Nuclear Science and Engineering grant ALNGRA15502 to HCB and an ANSTO Research grant AP 12760 to HJA. We thank Dr Samuel Toucanne (Ifremer) for providing a further radiocarbon date to improve the age modelling of the deglaciation. We acknowledge the financial support from the Australian Government to the Centre for Accelerator Science at ANSTO through the National Collaborative Research Infrastructure Strategy (NCRIS). We acknowledge the contributions of Bruce Hayward to temperature measurements and Gavin Foster for funding

of alkenone and Mg/Ca measurements. Lastly, we thank Bob Anderson for comments on an early draft, which greatly strengthened this manuscript.

Reference

Ahn, J., & Brook, E.J. 2008. "Atmospheric CO2 and Climate on Millennial Time Scales During the Last Glacial Period." *Science* 322: 83–85.

Anderson, H.J., Pedro, J.B., Bostock, H.C., Chase, Z., & Noble, T.L. 2021. "Compiled Southern Ocean Sea Surface Temperatures Correlate with Antarctic Isotope Maxima." *Quaternary Science Reviews* 255: 106821. https://doi.org/10.1016/j.quascirev.2021.106821.

Anderson, R.F., Ali, S., Bradtmiller, L.I., Nielsen, S.H.H., Fleisher, M.Q., Anderson, B.E., & Burckle, L.H. 2009. "Wind-Driven Upwelling in the Southern Ocean and the Degalcial Rise in Atmospheric CO2." *Science* 323: 1443–48.

Anderson, R.F., Barker, S., Fleisher, M., Gersonde, R., Goldstein, S.L., Kuhn, G., Mortyn, P.G., Pahnke, K., & Sachs, J.P. 2014. "Biological Response to Millennial Variability of Dust and Nutrient Supply in the Subantarctic South Atlantic Ocean." *Philosophical Transactions of the Royal Society A: Mathematical, Physical and Engineering Sciences* 372: 20130. https://doi.org/10.1098/rsta.2013.0054.

Bauska, T.K., Brook, E.J., Marcott, S.A., Baggenstos, D., Shackleton, S., Severinghaus, J.P., & Petrenko, V. V. 2018. "Controls on Millennial-Scale Atmospheric CO $_2$ Variability during the Last Glacial Period." *Geophysical Research Letters*, 7731–40. https://doi.org/10.1029/2018GL077881.

Belkin, I.M., & Gordon, A.L. 1996. "Southern Ocean Fronts from the Greenwich Meridian to Tasmania." *Journal of Geophysical Research* 101 (C2): 3675–96. https://doi.org/10.1029/95JC02750.

Bereiter, B., Luthi, D., Siegrist, M., Schupbach, S., Stocker, T.F., & Fischer, H. 2012. "Mode Change of Millennial CO2 Variability during the Last Glacial Cycle Associated with a Bipolar Marine Carbon Seesaw." *Proceedings of the National Academy of Sciences* 109 (25): 9755–60. https://doi.org/10.1073/pnas.1204069109.

Bereiter, Bernhard., Eggleston, S., Schmitt, J., Nehrbass-Ahles, C., Stocker, T.F., Fischer, H., Kipfstuhl, S., & Chappellaz, J. 2015. "Revision of the EPICA Dome C CO2 Record from 800 to 600-Kyr before Present." *Geophysical Research Letters* 42 (2): 542–49. https://doi.org/10.1002/2014GL061957.

Bohm, E., Lippold, J., Gutjahr, M., Frank, M., Blaser, P., Antz, B., Fohlmeister, J., Frank, N., Andersen, M.B., & Deininger, M. 2015. "Strong and Deep Atlantic Meridional Overturning Circulation during the Last Glacial Cycle." *Nature* 517 (7532): 73–76. https://doi.org/10.1038/nature14059.

Bostock, H.C., Hayward, B.W., Neil, H.L., Currie, K.I., & Dunbar, G.B. 2011. "Deep-Water Carbonate Concentrations in the Southwest Pacific."

Deep-Sea Research Part I: Oceanographic Research Papers 58 (1): 72–85. https://doi.org/10.1016/j.dsr.2010.11.010.

Bostock, H.C., Hayward, B.W., Neil, H.L., Sabaa, A.T., & Scott, G.H. 2015. "Changes in the Position of the Subtropical Front South of New Zealand since the Last Glacial Period." *Paleoceanography* 30 (7): 824–44. https://doi.org/10.1002/2014PA002652.

Buitenhuis, E.T., Pangerc, T., Franklin, D.J., Quéré, C. Le, & Malin, G. 2008. "Growth Rates of Six Coccolithophorid Strains as a Function of Temperature." *Limnology and Oceanography* 53 (3): 1181–85. https://doi.org/10.4319/lo.2008.53.3.1181.

Burke, A., Stewart, A.L., Adkins, J.F., Ferrari, R., Jansen, M.F., & Thompson, A.F. 2015. "The Glacial Mid-Depth Radiocarbon Bulge and Its Implications for the Overturning Circulation." *Paleoceanography* 30: 1021–39. https://doi.org/10.1002/2015PA002778.

Butzin, M., Köhler, P., & Lohmann, G. 2017. "Marine Radiocarbon Reservoir Age Simulations for the Past 50,000 Years." *Geophysical Research Letters* 44 (16): 8473–80. https://doi.org/10.1002/2017GL074688.

Carter, L., Neil, H.L., & McCave, I.N. 2000. "Glacial to Interglacial Changes in Non-Carbonate and Carbonate Accumulation in the SW Pacific Ocean, New Zealand." *Palaeogeography, Palaeoclimatology, Palaeoecology* 162 (3–4): 333–56. https://doi.org/10.1016/S0031-0182(00)00137-1.

Carter, L., & McCave, I. N. (2002). Eastern New Zealand drifts, Miocene-recent. *MEMOIRS-*

GEOLOGICAL SOCIETY OF LONDON, *22*, 385-408.

Carter, Lionel, McCave, I.N., & Williams, M.J.M. 2008. "Circulation and Water Masses of the Southern Ocean: A Review." In *Developments in Earth and Environmental Sciences*, 8:85–114. https://doi.org/10.1016/S1571-9197(08)00004-9.

Chase, Z., Anderson, R.F., Fleisher, M.Q., & Kubik, P.W. 2003. "Accumulation of Biogenic and Lithogenic Material in the Pacific Sector of the Southern Ocean during the Past 40,000 Years." *Deep-Sea Research Part II: Topical Studies in Oceanography* 50 (3–4): 799–832. https://doi.org/10.1016/S0967-0645(02)00595-7.

Chiang, J.C.H., Lee, S.Y., Putnam, A.E., & Wang, X. 2014. "South Pacific Split Jet, ITCZ Shifts, and Atmospheric North-South Linkages during Abrupt Climate Changes of the Last Glacial Period." *Earth and Planetary Science Letters* 406: 233–46. https://doi.org/10.1016/j.epsl.2014.09.012.

Chiswell, S.M., Bostock, H.C., Sutton, P.J.H., & Williams, M.J. 2015. "Physical Oceanography of the Deep Seas around New Zealand: A Review." *New Zealand Journal of Marine and Freshwater Research* 49 (2): 286–317. https://doi.org/10.1080/00288330.2014.992918.

Duncan, B., Carter, L., Dunbar, G., Bostock, H., Neil, H., Scott, G., Hayward, B.W., & Sabaa, A. 2016. "Interglacial/Glacial Changes in Coccolith-Rich Deposition in the SW Pacific Ocean: An Analogue for a Warmer World?" *Global and Planetary Change* 144: 252–62. https://doi.org/10.1016/j.gloplacha.2016.08.001.

Durand, A. 2017. "Ocean Deoxygenation, a Paleo-Proxy Perspective." PhD thesis, University of Tasmania, Hobart, Tasmania.

Durand, A., Chase, Z., Noble, T.L., Bostock, H., Jaccard, S.L., Kitchener, P., Townsend, A.T., et al., 2017. "Export Production in the New-Zealand Region since the Last Glacial Maximum." *Earth and Planetary Science Letters* 469: 110–22. https://doi.org/10.1016/j.epsl.2017.03.035.

Durand, A., Chase, Z., Townsend, A.T., Noble, T., Panietz, E., & Goemann, K. 2016. "Improved Methodology for the Microwave Digestion of Carbonate-Rich Environmental Samples." *International Journal of Environmental Analytical Chemistry* 96 (2): 119–36. https://doi.org/10.1080/03067319.2015.1137904.

Elderfield, H., & Ganssen, G. 2000. "Past Temperature and Δ18O of Surface Ocean Waters Inferred from Foraminiferal Mg/Ca Ratios." *Nature* 405 (6785): 442–45. https://doi.org/10.1038/35013033.

Ferrari, R., Jansen, M.F., Adkins, J.F., Burke, A., Stewart, A.L., & Thompson, A.F. 2014. "Antarctic Sea Ice Control on Ocean Circulation in Present and Glacial Climates." *Proceedings of the National Academy of Sciences of the United States of America* 111 (24): 8753–58. https://doi.org/10.1073/pnas.1323922111.

Francois, R., Frank, M., Rutgers van der Loeff, M.M., & Bacon, M.P. 2004. "Th Normalization: An Essential Tool for Interpreting Sedimentary Fluxes during the Late Quaternary." *Paleoceanography* 19 (1): 837–40. https://doi.org/10.1029/2003PA000939.

Garcia, H., Weathers, K.W., Paver, C.R., Smolyar, I., Boyer, T.P., Locarnini, R.A., Zweng, M.M., et al., 2018. "World Ocean Atlas 2018. Volume 4: Dissolved Inorganic Nutrients (Phosphate, Nitrate and Nitrate+nitrite, Silicate)." *NOAA Atlas NESDIS 84* 84 (July): 35.

Gottschalk, J., Skinner, L.C., Lippold, J., Vogel, H., Frank, N., Jaccard, S.L., & Waelbroeck, C. 2016. "Biological and Physical Controls in the Southern Ocean on Past Millennial-Scale Atmospheric CO2 Changes." *Nature Communications* 7 (May). https://doi.org/10.1038/ncomms11539.

Harris, P.G., & Maxwell, J.R. 1995. "A Novel Method for the Rapid Determination of Chlorin Concentrations at High Stratigraphic Resolution in Marine Sediments." *Organic Geochemistry* 23 (9): 853–56. https://doi.org/10.1016/0146-6380(95)80007-E.

Hayward, B.W., Sabaa, A.T., Kolodziej, A., Crundwell, M.P., Steph, S., Scott, G.H., Neil, H.L., Bostock, H.C., Carter, L., & Grenfell, H.R. 2012.

"Planktic Foraminifera-Based Sea-Surface Temperature Record in the Tasman Sea and History of the Subtropical Front around New Zealand, over the Last One Million Years." *Marine Micropaleontology* 82–83: 13–27. https://doi.org/10.1016/j.marmicro.2011.10.003.

Heaton, T.J., Köhler, P., Butzin, M., Bard, E., Reimer, R.W., Austin, W.E.N., Bronk Ramsey, C., et al., 2020. "Marine20 - The Marine Radiocarbon Age Calibration Curve (0-55,000 Cal BP)." *Radiocarbon* 62 (4): 779–820. https://doi.org/10.1017/RDC.2020.68.

Hedges, J.I., & Stern, J.H. 1984. "Carbon and Nitrogen Determinations of Carbonate-Containing Solids." *Limnology and Oceanography* 29 (3): 663–66.

Henderson, G.M., & Anderson, 2003. "The U-Series Toolbox for Paleoceanography." *Reviews in Mineralogy and Geochemistry* 52 (1): 493–531. https://doi.org/10.2113/0520493.

Higginson, M.J., Maxwell, J.R., & Altabet, M.A. 2003. "Nitrogen Isotope and Chlorin Paleoproductivity Records from the Northern South China Sea: Remote vs. Local Forcing of Millennial- and Orbital-Scale Variability." *Marine Geology* 201 (1–3): 223–50. https://doi.org/10.1016/S0025-3227(03)00218-4.

Howard, W.R., & Prell, W.L. 1994. "Late Quaternary CaCO3 Production and Preservation in the Southern Ocean: Implications for Oceanic and Atmospheric Carbon Cycling." *Paleoceanography* 9 (3): 453–82.

Hutchins, D.A., Sedwick, P.N., Ditullio, G.R., Boyd, P.W., Queguiner, B., Griffiths, F.B., & Crossley, C. 2001. "Control of Phytoplankton Growth by Iron Supply and Irradiance in the Subantarctic Southern Ocean: Experimental Results from the SAZ Project." *Journal of Geophysical Research: Oceans* 106 (C12): 31573–83. https://doi.org/10.1029/2000jc000348.Jaccard, S.L., Galbraith, E.D., Martínez-Garciá, A., & Anderson, R.F. 2016. "Covariation of Deep Southern Ocean Oxygenation and Atmospheric CO2 through the Last Ice Age." *Nature* 530 (7589): 207–10. https://doi.org/10.1038/nature16514.Jaccard, S.L., Hayes, C.T., Martínez-Garcia, A., Hodell, D. a, Anderson, R.F., Sigman, D.M., & Haug, G.H. 2013. "Two Modes of Change in Southern Ocean Productivity over the Past Million Years." *Science* 339 (6126): 1419–23. https://doi.org/10.1126/science.1227545.Jones, G.A., & Kaiteris, P. 1983. "A Vacuum-Gasometric Technique for Rapid and Precise Analysis of Calcium Carbonate in Sediments and Soils." *Journal of Sedimentary Research* 53 (2): 655–60. https://doi.org/10.1306/212f825b-2b24-11d7-8648000102c1865d.Jouzel, J., Masson-Delmotte, V., Cattani, O., Dreyfus, G., Falourd, S., Hoffmann, G., Minster, B., et al., 2007. "EPICA Dome C Ice Core 800kyr Deuterium Data and Temperature Estimates." IGBP PAGES/World Data Center for Paleoclimatology Data Contribution Series. 2007.Kawano, T., Fukasawa, M., Kouketsu, S., Uchida, H., Doi, T., Kaneko, I., Aoyama, M., & Schneider, W. 2006. "Bottom Water Warming along the Pathway of Lower Circumpolar Deep Water in the Pacific Ocean." *Geophysical Research Letters* 33 (23): 2–6. https://doi.org/10.1029/2006GL027933.Kienast,

S.S., Winckler, G., Lippold, J., Albani, S., & Mahowald, N.M. 2016. "Tracing Dust Input to the Global Ocean Using Thorium Isotopes in Marine Sediments: ThoroMap." *Global Biogeochemical Cycles* 30 (10): 1526–41. https://doi.org/10.1002/2016GB005408.Krumhardt, K.M., Lovenduski, N.S., Iglesias-Rodriguez, M.D., & Kleypas, J.A. 2017. "Coccolithophore Growth and Calcification in a Changing Ocean." *Progress in Oceanography* 159 (June): 276–95. https://doi.org/10.1016/j.pocean.2017.10.007.Lamy, F., Gersonde, R., Winckler, G., Esper, O., Jaeschke, A., Kuhn, G., Ullermann, J., Martinez-Garcia, A., Lambert, F., & Kilian, R. 2014. "Increased Dust Deposition in the Pacific Southern Ocean During Glacial Periods." *Science* 343 (January): 403–7. https://doi.org/10.4159/harvard.9780674430501.c21.Lauvset, S.K., Olsen, A., Lange, N., Key, R.M., Tanhua, T., Bittig, H.C., Kozyr, A., et al., 2020. "An Updated Version of the Global Interior Ocean Biogeochemical Data Product, GLODAPv2.2020." *Earth System Science Data* 12 (4): 3653–78. https://doi.org/10.5194/essd-12-3653-2020.Leblanc, K., Hare, C.E., Boyd, P.W., Bruland, K.W., Sohst, B., Pickmere, S., Lohan, M.C., Buck, K., Ellwood, M., & Hutchins, D.A. 2005. "Fe and Zn Effects on the Si Cycle and Diatom Community Structure in Two Contrasting High and Low-Silicate HNLC Areas." *Deep-Sea Research Part I: Oceanographic Research Papers* 52 (10): 1842–64. https://doi.org/10.1016/j.dsr.2005.06.005.Lougheed, B.C., & Obrochta, S.P. 2019. "A Rapid, Deterministic Age-Depth Modeling Routine for Geological Sequences With Inherent Depth Uncertainty." *Paleoceanography and Paleoclimatology* 34 (1): 122–33. https://doi.org/10.1029/2018PA003457.Marr, J.P., Carter, L., Bostock, H.C., Bolton, A., & Smith, E. 2013. "Southwest Pacific Ocean Response to a Warming World: Using Mg/Ca, Zn/Ca, and Mn/Ca in Foraminifera to Track Surface Ocean Water Masses during the Last Deglaciation." *Paleoceanography* 28 (2): 347–62. https://doi.org/10.1002/palo.20032.Martínez-Garcia, A., Rosell-Melé, A., Geibert, W., Gersonde, R., Masqué, P., Gaspari, V., & Barbante, C. 2009. "Links between Iron Supply, Marine Productivity, Sea Surface Temperature, and CO2 over the Last 1.1 Ma." *Paleoceanography* 24 (1): 1–14. https://doi.org/10.1029/2008PA001657.Martínez-Garcia, A., Rosell-Melé, A., Jaccard, S.L., Geibert, W., Sigman, D.M., & Haug, G.H. 2011. "Southern Ocean Dust-Climate Coupling over the Past Four Million Years." *Nature* 476 (7360): 312–15. https://doi.org/10.1038/nature10310.Martínez-García, A., Sigman, D.M., Ren, H., Anderson, R.F., Straub, M., Hodell, D.A., Jaccard, S.L., Eglinton, T.I., & Haug, G.H. 2014. "Iron Fertilization of the Subantarctic Ocean During the Last Ice Age." *Science* 343: 1347–50.McCave, I.N., Carter, L., & Hall, I.R. 2008. "Glacial-Interglacial Changes in Water Mass Structure and Flow in the SW Pacific Ocean." *Quaternary Science Reviews* 27 (19–20): 1886–1908. https://doi.org/10.1016/j.quascirev.2008.07.010.Menviel, L., England, M.H., Meissner, K.J., Mouchet, A., & Yu, J. 2014. "Atlantic-Pacific Seesaw and Its Role in Outgassing CO2 during Heinrich Events." *Paleoceanography* 29 (1): 58–70. https://doi.org/10.1002/2013PA002542.Noble, T.L., Piotrowski, A.M., & McCave, I.N. 2013. "Neodymium Isotopic Composition of Intermediate and Deep Waters in the Glacial Southwest Pacific." *Earth and Planetary*

Science Letters 384: 27–36. https://doi.org/10.1016/j.epsl.2013.10.010.Orsi, A.H., Whitworth, T., & Nowlin, W.D. 1995. "On the Meridional Extent and Fronts of the Antarctic Circumpolar Current." *Deep-Sea Research Part I* 42 (5): 641–73. https://doi.org/10.1016/0967-0637(95)00021-W.Pahnke, K., & Zahn, R. 2005. "Southern Hemishphere Water Mass Conversion Linked with North Atlantic Climate Variability." *Science* 307 (March): 1741–47.Pavia, F.J., Wang, S., Middleton, J., Murray, R.W., & Anderson, R.F. 2021. "Trace Metal Evidence for Deglacial Ventilation of the Abyssal Pacific and Southern Oceans." *Paleoceanography and Paleoclimatology* 36 (9): 1–15. https://doi.org/10.1029/2021pa004226.Pedro, J.B., Martin, T., Steig, E.J., Jochum, M., Park, W., & Rasmussen, S.O. 2016. "Southern Ocean Deep Convection as a Driver of Antarctic Warming Events." *Geophysical Research Letters* 43 (5): 2192–99. https://doi.org/10.1002/2016GL067861.Peloquin, J., Hall, J., Safi, K., Smith, W.O., Wright, S., & Enden, R. van den. 2011. "The Response of Phytoplankton to Iron Enrichment in Sub-Antarctic HNLCLSi Waters: Results from the SAGE Experiment." *Deep-Sea Research Part II: Topical Studies in Oceanography* 58 (6): 808–23. https://doi.org/10.1016/j.dsr2.2010.10.021.Ren, H., Sigman, D.M., Martínez-García, A., Anderson, R.F., Chen, M. Te, Ravelo, A.C., Straub, M., Wong, G.T.F., & Haug, G.H. 2017. "Impact of Glacial/Interglacial Sea Level Change on the Ocean Nitrogen Cycle." *Proceedings of the National Academy of Sciences of the United States of America* 114 (33): E6759–66. https://doi.org/10.1073/pnas.1701315114.Robinson, R.S., & Sigman, D.M. 2008. "Nitrogen Isotopic Evidence for a Poleward Decrease in Surface Nitrate within the Ice Age Antarctic." *Quaternary Science Reviews* 27 (9–10): 1076–90. https://doi.org/10.1016/j.quascirev.2008.02.005.Robinson, R.S., Sigman, D.M., DiFiore, P.J., Rohde, M.M., Mashiotta, T.A., & Lea, D.W. 2005. "Diatom-Bound 15N/14N: New Support for Enhanced Nutrient Consumption in the Ice Age Subantarctic." *Paleoceanography* 20 (3): 1–14. https://doi.org/10.1029/2004PA001114.Ronge, T.A., Lippold, J., Geibert, W., Jaccard, S.L., Schnülle, S.M., Süfke, F., & Tiedemann, R. 2021. "Deglacial Patterns of South Pacific Overturning Inferred from 231Pa and 230Th." *Nature Scientific Reports* 11 (20473): 1–11. https://doi.org/10.1038/s41598-021-00111-1.Ronge, T.A., Steph, S., Tiedemann, R., Prange, M., Merkel, U., Nürnberg, D., & Kuhn, G. 2015. "Pushing the Boundaries: Glacial/Interglacial Variability of Intermediate and Deep Waters in the Southwest Pacific over the Last 350,000 Years." *Paleoceanography* 30 (2): 23–38. https://doi.org/10.1002/2014PA002727.Rudnick, R.L., & Gao, S. 2003. "Composition of the Continental Crust." In *The Crust*.Sachs, J.P., & Anderson, R.F. 2005. "Increased Productivity in the Subantarctic Ocean during Heinrich Events." *Nature* 434 (7037): 1118–21. https://doi.org/10.1038/nature03544.Shoenfelt, E.M., Winckler, G., Lamy, F., Anderson, R.F., & Bostick, B.C. 2018. "Highly Bioavailable Dust-Borne Iron Delivered to the Southern Ocean during Glacial Periods." *Proceedings of the National Academy of Sciences of the United States of America* 115 (44): 11180–85. https://doi.org/10.1073/pnas.1809755115.Shulmeister, J., Thackray, G.D., Rittenour, T.M., Fink, D., & Patton, N.R. 2019. "The Timing and

Nature of the Last Glacial Cycle in New Zealand." *Quaternary Science Reviews* 206: 1–20. https://doi.org/10.1016/j.quascirev.2018.12.020.Shulmeister, J., Thackray, G.D., Rittenour, T.M., & Hyatt, O.M. 2018. "Multiple Glacial Advances in the Rangitata Valley, South Island, New Zealand, Imply Roles for Southern Hemisphere Westerlies and Summer Insolation in MIS 3 Glacial Advances." *Quaternary Research (United States)* 89 (2): 375–93. https://doi.org/10.1017/qua.2017.108.Shuttleworth, R., Bostock, H.C., Chalk, T.B., Calvo, E., Jaccard, S.L., Pelejero, C., Martínez-García, A., & Foster, G.L. 2021. "Early Deglacial CO2 Release from the Sub-Antarctic Atlantic and Pacific Oceans." *Earth and Planetary Science Letters* 554: 116649. https://doi.org/10.1016/j.epsl.2020.116649.Sigman, D.M., Altabet, M.A., McCorkle, D.C., Francois, R., & Fischer, G. 1999. "The Δ15N of Nitrate in the Southern Ocean: Consumption of Nitrate in Surface Waters." *Global Biogeochemical Cycles* 13 (4): 1149–66. https://doi.org/10.1029/1999GB900038.Sigman, D.M., Hain, M.P., & Haug, G.H. 2010. "The Polar Ocean and Glacial Cycles in Atmospheric CO2 Concentration." *Nature* 466 (7302): 47–55. https://doi.org/10.1038/nature09149.Sikes, E.L., & Sicre, M.-A. 2002. " Relationship of the Tetra-Unsaturated C 37 Alkenone to Salinity and Temperature: Implications for Paleoproxy Applications ." *Geochemistry, Geophysics, Geosystems* 3 (11): 1–11. https://doi.org/10.1029/2002gc000345.Skinner, L.C., Menviel, L., Broadfield, L., Gottschalk, J., & Greaves, M. 2020. "Southern Ocean Convection Amplified Past Antarctic Warming and CO2 Rise during Heinrich Stadial 4." *Communications Earth and Environment* 1 (23): 1–8. https://doi.org/10.1038/s43247-020-00024-3.Smith, R.O., Vennell, R., Bostock, H.C., & Williams, M.J.M. 2013. "Interaction of the Subtropical Front with Topography around Southern New Zealand." *Deep-Sea Research Part I: Oceanographic Research Papers* 76: 13–26. https://doi.org/10.1016/j.dsr.2013.02.007.Stephens, B.B., & Keeling, R.F. 2000. "The Influence of Antarctic Sea Ice on Glacial-Interglacial CO2 Variations." *Nature* 404 (6774): 171–74. https://doi.org/10.1038/35004556.Talley, L.D. 2013. "Closure of the Global Overturning Circulation through the Indian, Pacific, and Southern Oceans." *Oceanography* 26 (1): 80–97. https://doi.org/10.5670/oceanog.2013.07.Thöle, L.M., Amsler, H.E., Moretti, S., Auderset, A., Gilgannon, J., Lippold, J., Vogel, H., et al., 2019. "Glacial-Interglacial Dust and Export Production Records from the Southern Indian Ocean." *Earth and Planetary Science Letters* 525: 115716. https://doi.org/10.1016/j.epsl.2019.115716.Toggweiler, J.R., Russell, J.L., & Carson, S.R. 2006. "Midlatitude Westerlies, Atmospheric CO2, and Climate Change during the Ice Ages." *Paleoceanography* 21 (2): 1–15. https://doi.org/10.1029/2005PA001154.Trudgill, M.D., Shuttleworth, R., Bostock, H.C., Burke, A., Cooper, M.J., Greenop, R., & Foster, G.L. 2020. "The Flux and Provenance of Dust Delivered to the SW Pacific During the Last Glacial Maximum Paleoceanography and Paleoclimatology." *Paleoceanography and Paleoclimatology* 35: 1–17. https://doi.org/10.1029/2020PA003869.Veres, D., Bazin, L., Landais, A., Toyé Mahamadou Kele, H., Lemieux-Dudon, B., Parrenin, F., Martinerie, P., et al., 2013. "The Antarctic Ice Core

Chronology (AICC2012): An Optimized Multi-Parameter and Multi-Site Dating Approach for the Last 120 Thousand Years." *Climate of the Past* 9 (4): 1733–48. https://doi.org/10.5194/cp-9-1733-2013.Wang, X.T., Sigman, D.M., Prokopenko, M.G., Adkins, J.F., Robinson, L.F., Hines, S.K., Chai, J., et al., 2017. "Deep-Sea Coral Evidence for Lower Southern Ocean Surface Nitrate Concentrations during the Last Ice Age." *Proceedings of the National Academy of Sciences of the United States of America* 114 (13): 3352–57. https://doi.org/10.1073/pnas.1615718114.Ziegler, M., Diz, P., Hall, I.R., & Zahn, R. 2013. "Millennial-Scale Changes in Atmospheric CO2 Levels Linked to the Southern Ocean Carbon Isotope Gradient and Dust Flux." *Nature Geoscience* 6 (6): 457–61. https://doi.org/10.1038/ngeo1782.

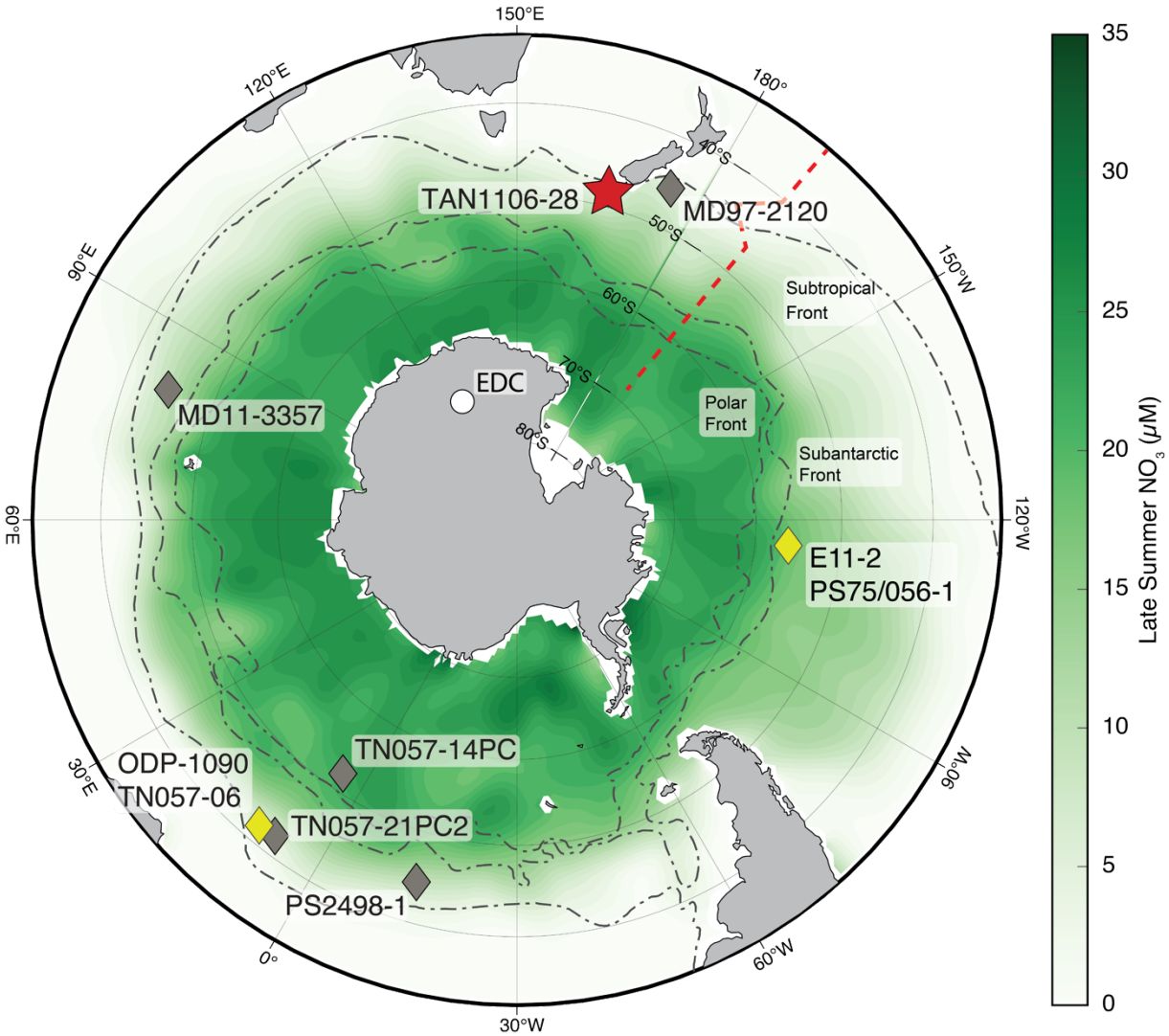

Figure 1. Modern February surface NO_3 concentration in Southern Ocean surface waters from World Ocean Atlas 2018 (Garcia et al., 2018). Red star represents the location of TAN1106-28 in the subantarctic Pacific Ocean. Grey diamonds represent published high-resolution export production or lithogenic 'dust' flux paleo-reconstructions that use the ^{230}Th normalisation method and span the majority of MIS-3. The yellow diamonds represent the existence of both the ^{230}Th-normalisation method and microfossil bound ^{15}N. White circle is the location of the EDC ice core. Red dashed line indicates position of P15S survey line used in Figure 2.

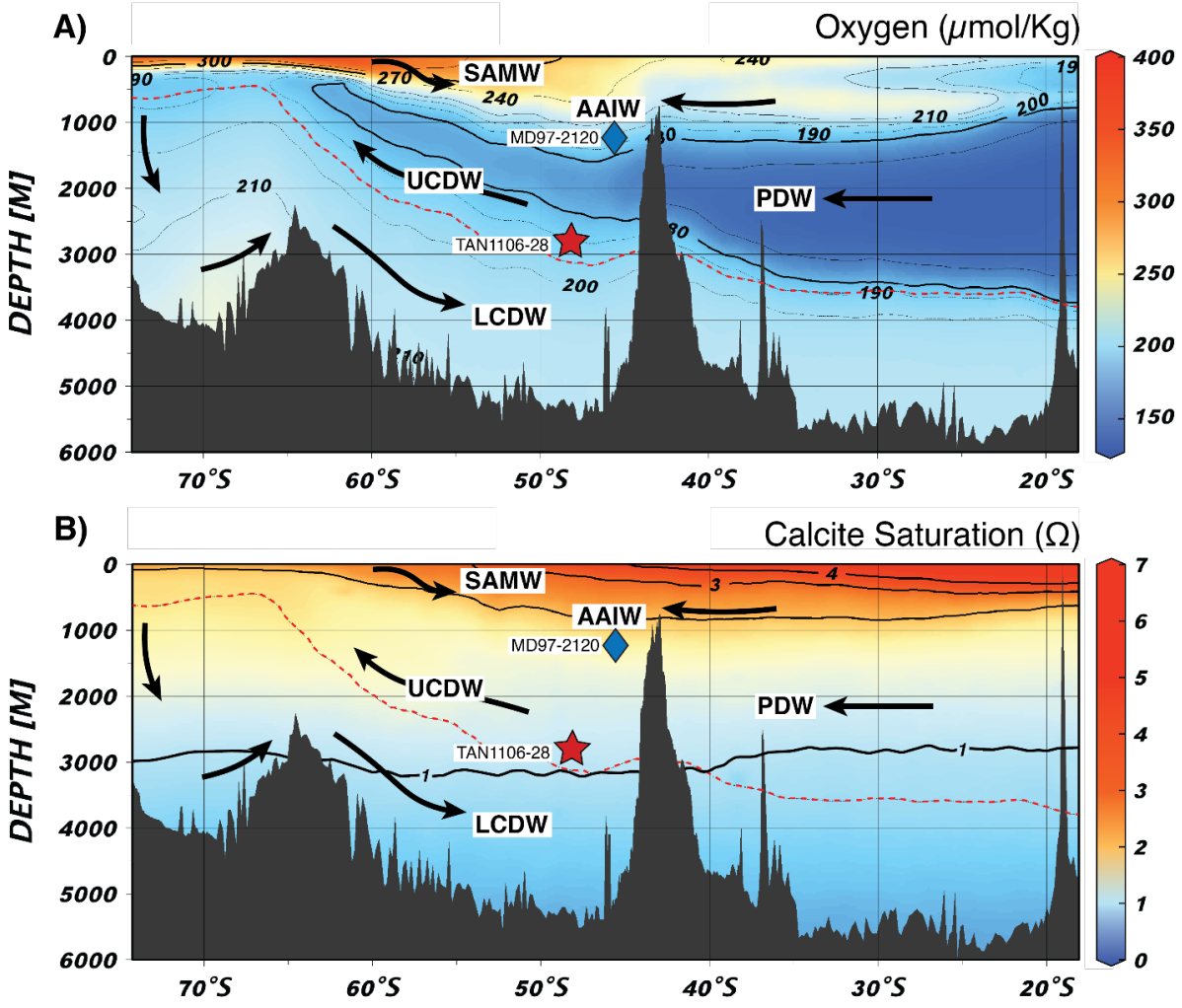

Figure 2. Modern cross sections through the WOCE P15S transect showing A) Oxygen concentrations, and B) calcite saturation state southwest Pacific (Lauvset et al., 2020) – blue diamond represents location of MD97-2120 (Sachs &

Anderson, 2005), red star represents TAN1106-28. SAMW = Subantarctic Mode Water, AAIW = Antarctic Intermediate Water, UCDW = Upper Circumpolar Deep Water, LCDW = Circumpolar Deep Water, and PDW = Pacific Deep Water. Red dashed line indicates the boundary between UCDW and LCDW. Note TAN1106-28 sits just to the west of the P15S section (Figure 1) but is similarly bathed in UCDW. Flow directions are inferred from Kawano et al., (2006) and Talley, (2013).

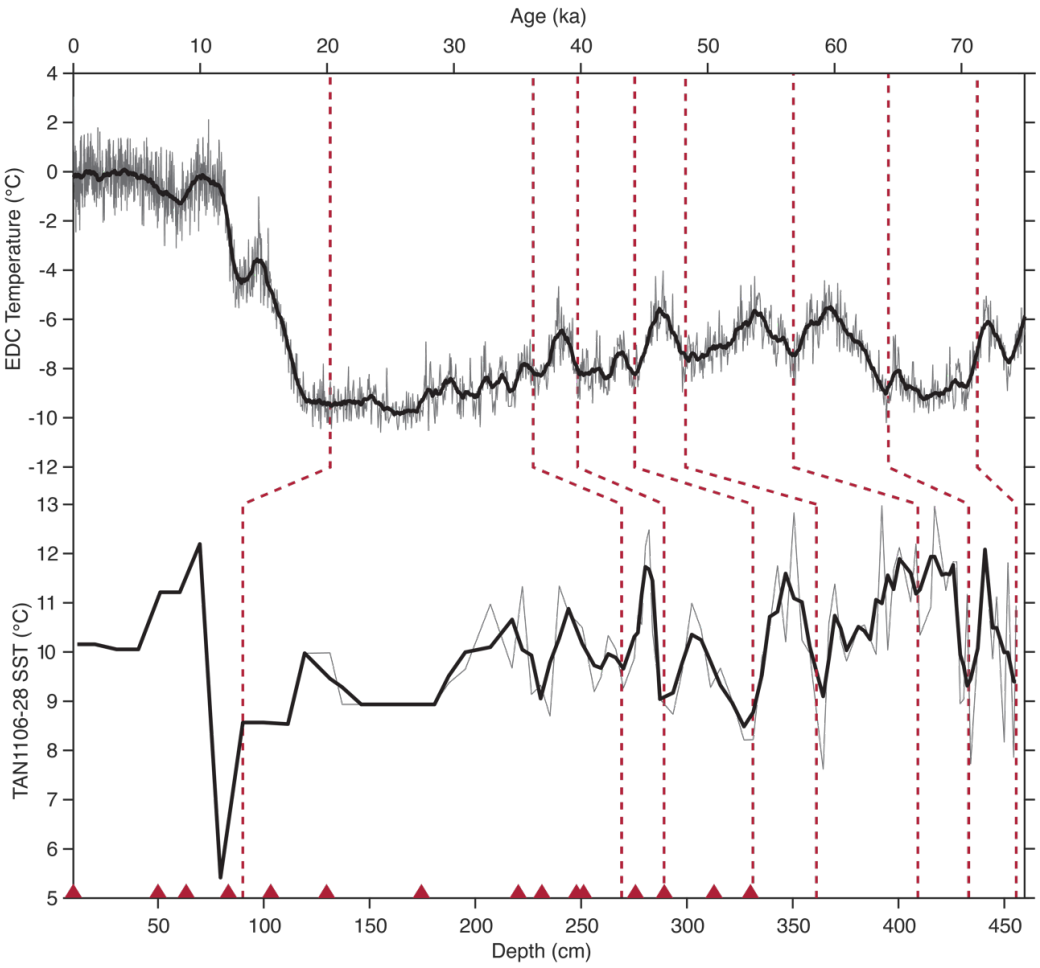

Figure 3. Top) EDC temperature record on the AICC2012 timescale (Jouzel et al., 2007; Veres et al., 2013), and bottom) mean SST at TAN1106-28 grey line is the three-proxy SST mean and black line is the 500-yr running mean. Dashed lines represent age control points between the two records, red triangles represent the depth of planktonic ^{14}C ages at TAN1106-28.

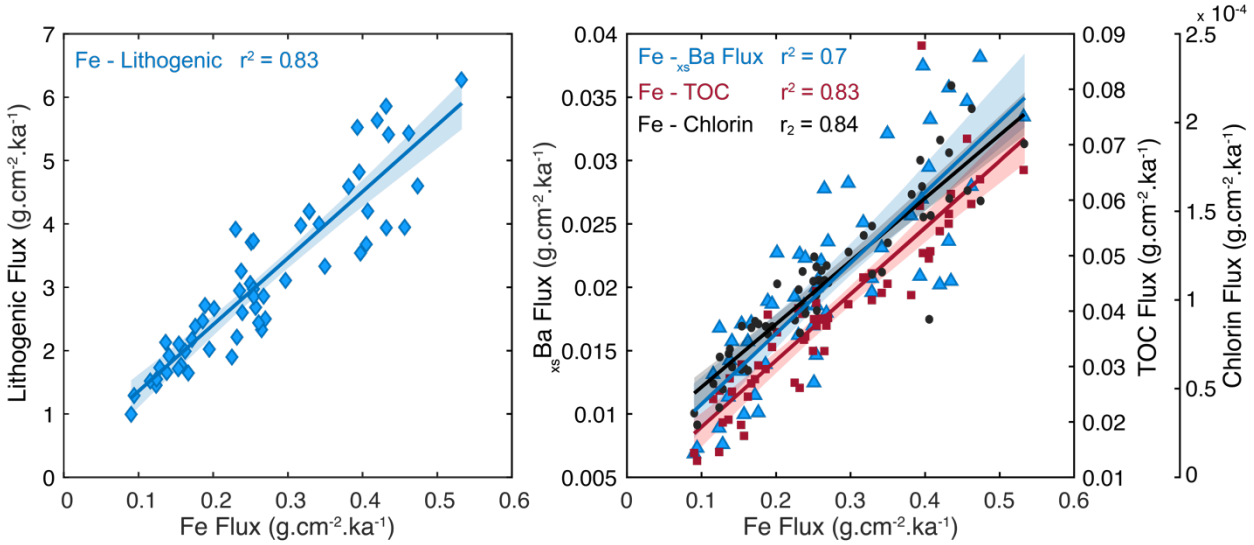

Figure 4. Left) linear regression between lithogenic material (blue) and iron fluxes, used to infer a continental origin for iron at TAN1106-28. Right) linear regression between export production fluxes; $_{xs}$Ba (blue) and TOC (red), and Chlorins with iron flux. Strong correlations support a lithogenic source of iron, and an effect of iron fertilisation on export production.

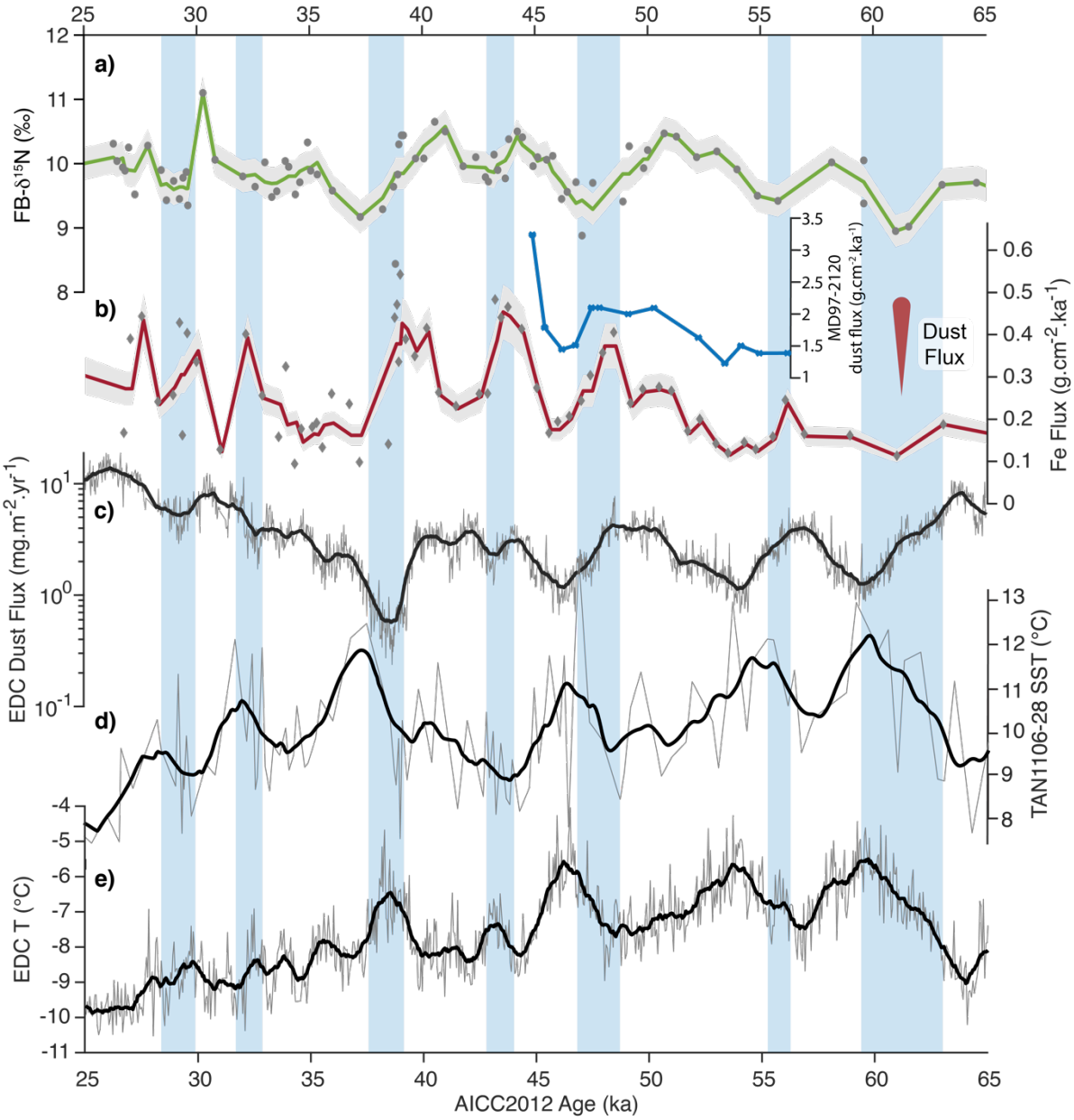

Figure 5. Proxies of lithogenic flux and nitrogen supply at TAN1106-28, (a) foraminiferal bound ^{15}N, (b) Fe flux (red) and the MD97-2120 lithogenic flux on the AIM-tuned timescale (Anderson et al., 2021), (c) EDC dust flux (Lambert et al., 2012), (d) black line 1000-yr running mean of the TAN1106-28 SST mean, and (e) grey line is the Antarctic temperature anomaly (Jouzel et al., 2007) with black line as the 500-yr running mean. Coloured lines for TAN1106-28

proxies represent the 500-yr running mean, grey envelopes represent the 1 error for each proxy. Vertical blue shading represents periods of increasing SST at TAN1106-28 that coincide with AIM events 17, 14, 12, 11, 8, 6, and 4. Antarctic records are on the AICC2012 timescale, and TAN1106-28 proxies are tied to the AICC2012 timescale (Veres et al., 2013).

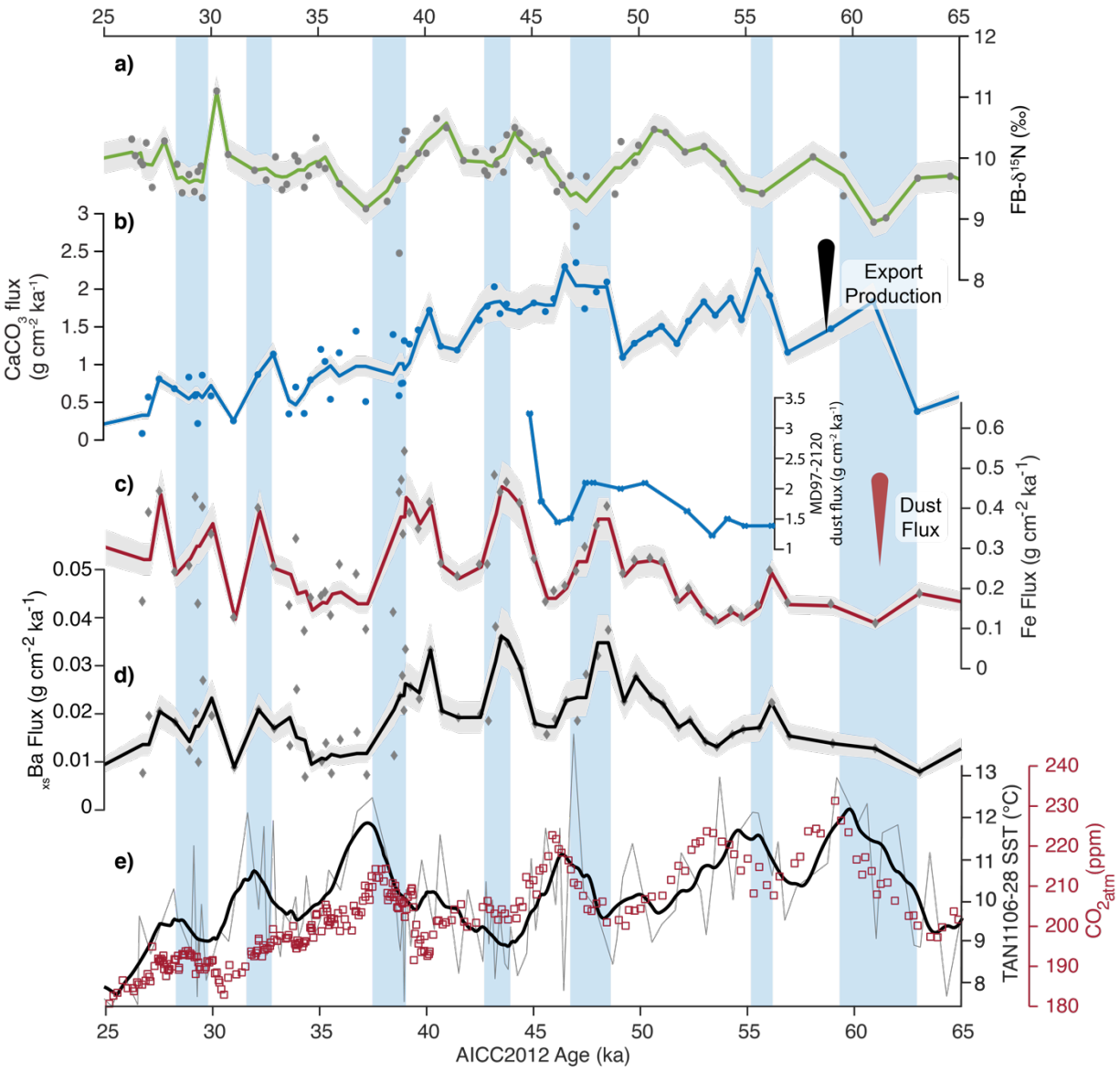

Figure 6. Proxies of iron flux and export production at TAN1106-28, (a) foraminiferal bound ^{15}N, (b) TAN1106-28 Calcium carbonate flux (blue) and MD97-2120 calcium carbonate flux (inset-blue) on the AIM-tuned age model

of Anderson et al., (2021), (c) iron flux (red), (d) $_{xs}$Ba flux (black), and (e) authigenic uranium concentrations at TAN1106-28 (red) and at MD97-2120 (blue) on the AIM-tuned age model of Anderson et al., (2021), and (e) thick black line is the 1000-yr running mean of the TAN1106-28 SST mean, thin grey line is SST variability, and red squares Composite Antarctic CO_2 (Bereiter et al., 2015). Coloured lines for TAN1106-28 proxies represent the 500-yr running mean at the site, grey envelopes represent the 1 error for each proxy. Vertical blue shading represents periods of increasing SST at TAN1106-28 that coincide with AIM events 17, 14, 12, 11, 8, 6, and 4. Antarctic records are on the AICC2012 timescale, and TAN1106-28 proxies are tied to the AICC2012 timescale (Veres et al., 2013).

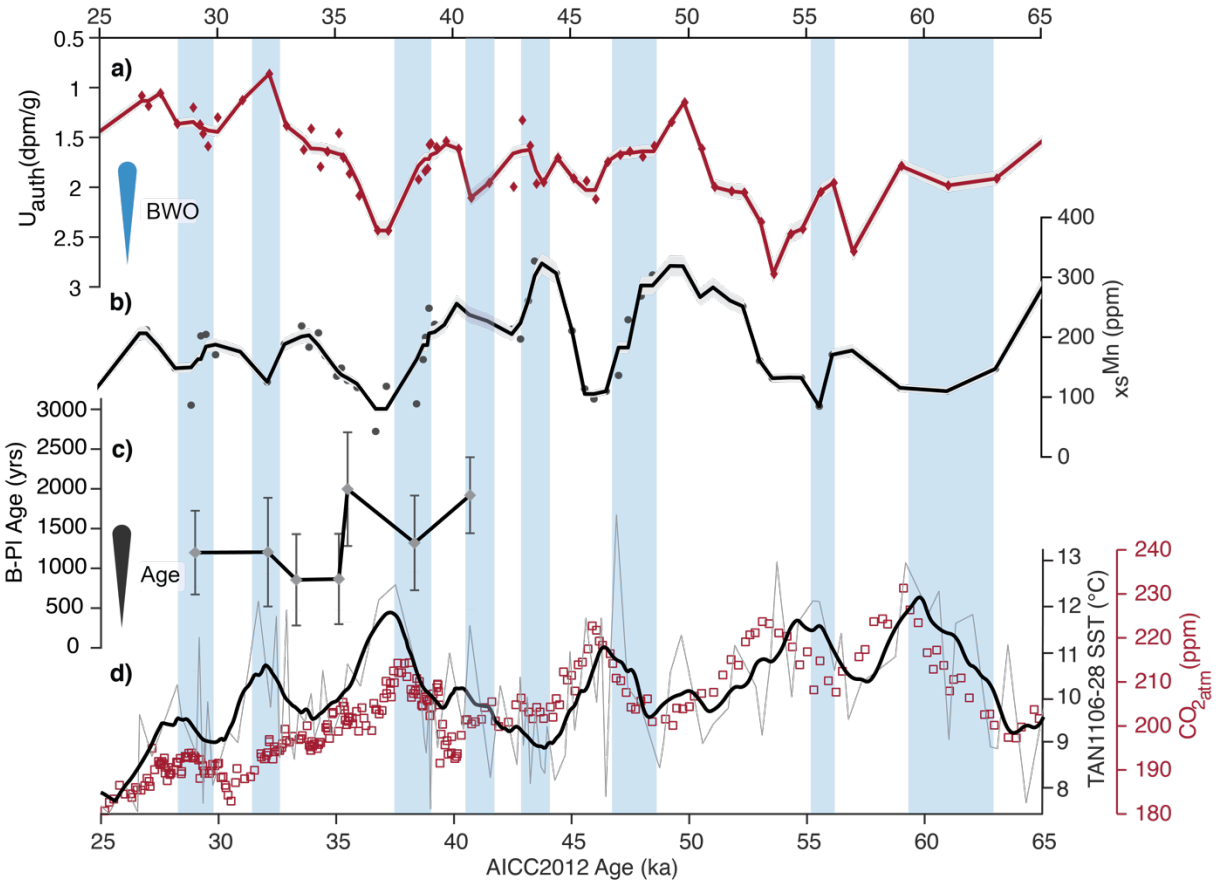

Figure 7. Bottom water oxygenation (BWO) and bottom water ages at TAN1106-28. a) xsMn concentrations, b) concentrations at TAN1106-28 U_{auth} in the southwest Pacific (blue — MD97-2120; Sachs & Anderson, 2005), c) paired Benthic–Planktic radiocarbon age offset (black), error bars represent the 2 error (note that dates from samples at 298.5cm and 313.5cm are removed as benthic ages are younger than the corresponding planktic age here) and d)

thick black line is the 1000-yr running mean of the TAN1106-28 SST mean, thin grey line is SST variability, and red squares Composite Antarctic CO_2 (Bereiter et al., 2015). Vertical blue shading represents periods of time with increasing SST that coincide with AIM events 17, 14, 12, 11, 10, 8, 6, and 4. Antarctic records are on the AICC2012 timescale, and TAN1106-28 proxies are tied to the AICC2012 timescale (Veres et al., 2013).

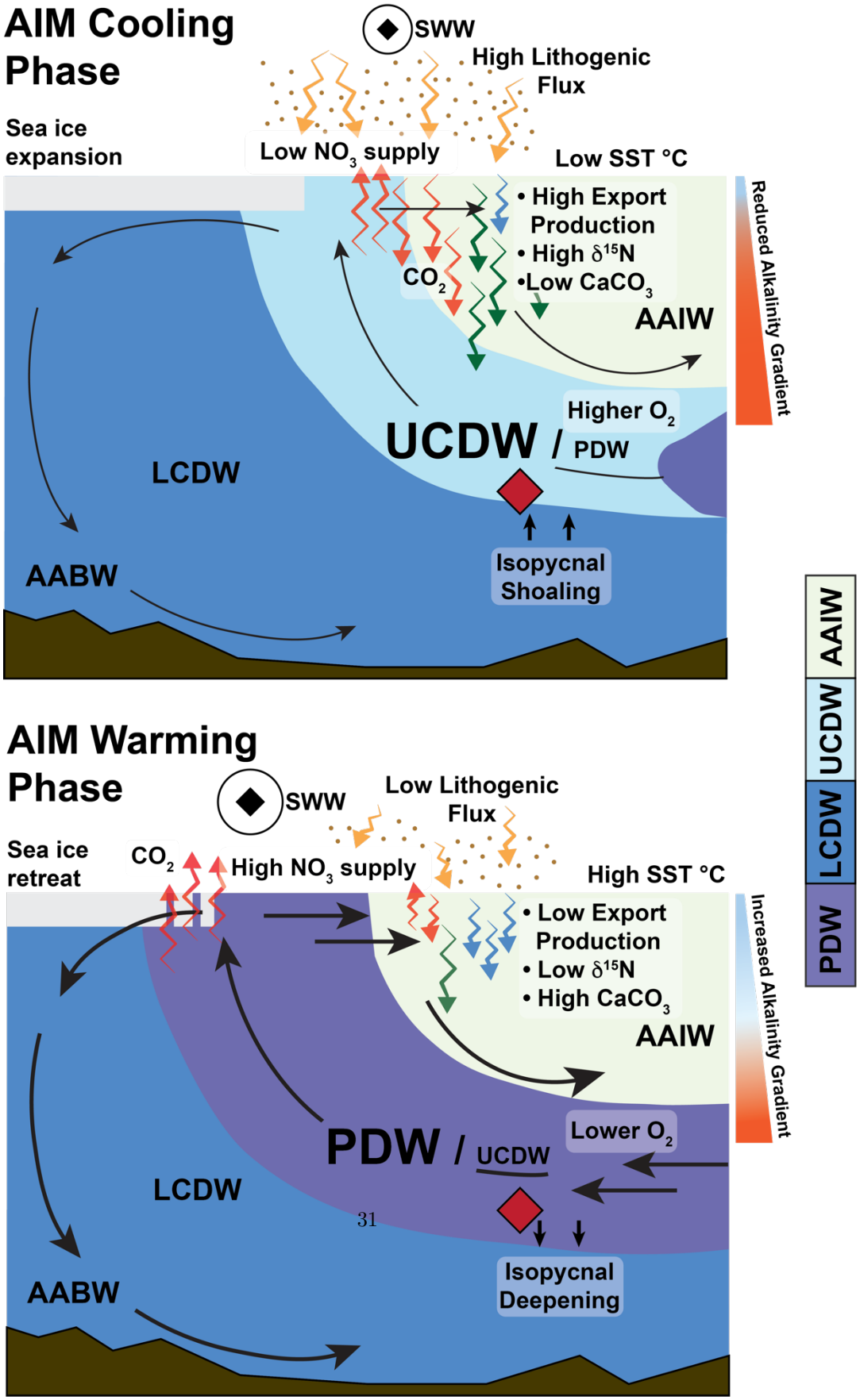
AIM Cooling Phase
SWW
High Lithogenic Flux
Sea ice expansion
Low NO3 supply
Low SST °C
• High Export Production
• High δ15N
•Low CaCO3
CO2
AAIW
Reduced Alkalinity Gradient
Higher O2
UCDW / PDW
LCDW
AABW
Isopycnal Shoaling
AIM Warming Phase
SWW
Low Lithogenic Flux
Sea ice retreat
CO2
High NO3 supply
High SST °C
• Low Export Production
• Low δ15N
• High CaCO3
AAIW
Increased Alkalinity Gradient
Lower O2
PDW / UCDW
LCDW
AABW
Isopycnal Deepening
AAIW
UCDW
LCDW
PDW

Figure 8. Previous page. Schematic cross section of the subantarctic southwest Pacific Ocean during millennial-scale changes of late MIS-3 based on this study and published proxy results (Anderson et al., 2009; Pavia et al., 2021; Ronge et al., 2021) and numerical modelling (Menviel et al., 2014). Top) during the AIM cooling phase SST decreases and a northward position SWW increases glaciogenic lithogenic material and iron flux to the surface ocean driving export production and nitrate utilisation. Increases in particulate organic carbon result in decreases in $CaCO_3$ flux and a reduced alkalinity gradient, increasing CO_2 drawdown. Decreased iron limitation increases the biological pump efficiency and CO_2 draw down while cool temperatures increase the solubility pump, simultaneously a isopycnal shoaling and a strong AMOC results in circumpolar deep water (LCDW) influencing the region, northward positioned SWW places reduces upwelling in the antarctic SO, NO_3 supply is reduced and utilisation increases both increasing FB- ^{15}N. Bottom) AIM warming phase, increased SST and reduced solubility pump, southward shifted SWW reduces glaciation and lithogenic material and iron flux, which in turn reduces export production, and nitrate utilisation. Reduced export production reduces biological pump efficiency and CO_2 drawdown, while increased $CaCO_3$ flux increases the alkalinity gradient between the surface and deep waters, further reducing CO_2 drawdown. Southward shift of Southern Ocean fronts and SWW increase supply of NO_3 to the subantarctic during all MIS-3 AIM warming events, decreasing subantarctic ^{15}N. Upwelling in the Southern Ocean increases due to an intensification of SWW, which stimulates Southern Ocean overturning. Isopycnal deepening and strengthened overturning drives an expansion of PDW over the TAN1106-28 core site, and SO upwelling contributes to outgassing of deep stored CO_2 to the atmosphere via air-sea gas exchange due to reduced sea-ice extent, while simultaneously reduced AMOC strength decreases the influence of CDW in the region. Red diamond indicates position of TAN1106-28, thin black lines indicate weaker transport, thick black lines indicate strengthened overturning. Early MIS-3 not shown in schematic but is characterised by reduced iron flux and export production.

Table 1. Next Page Planktic foraminiferal radiocarbon measurements and tie points to the EDC temperature record used for age modelling, and Benthic foraminiferal radiocarbon measurements (shaded grey) at TAN1106-28 used for deep water age offsets. NZA samples were previously published in Bostock et al., (2015), OZ samples were analysed at ANSTO, and AWI samples were analysed at the Alfred Wegener Institute.

Name	Type	Depth (cm)	^{14}C Yrs (ka BP, 1 error)	Reservoir Age (ka)	Mean Calibrated Age (ka cal BP, 95.4% C.I)
NZA 54355	**Planktic 14C**		± 0.02	± 0.1	± 0.14
NZA 54358	**Planktic 14C**		± 0.03	± 0.1	± 0.2
AWI 4559.1	**Planktic 14C**		± 0.04	± 0.1	± 0.18
NZA 54357	**Planktic 14C**		± 0.05	± 0.2	± 0.23
SST-1	**Tie point**		± 0.48	-	± 0.99
AWI 4550	**Planktic 14C**		± 0.05	± 0.2	± 0.28
OZT819	**Planktic 14C**		± 0.07	± 0.2	± 0.25
OZU082	**Planktic 14C**		± 0.08	± 0.2	± 0.23
SST-2	**Tie point**		± 0.36	-	± 1.03
OZAB77	**Planktic 14C**		± 0.08	± 0.2	± 0.21
OZT820	**Planktic 14C**		± 0.1	± 0.2	± 0.27
OZAB78	**Benthic 14C**		± 0.11	± 0.2	± 0.25
OZA073	**Planktic 14C**		± 0.17	± 0.2	± 0.28
OZT825	**Planktic 14C**		± 0.12	± 0.2	± 0.38
OZAB79‡	**Benthic 14C**		± 0.15	± 0.2	± 0.30
OZT821	**Planktic 14C**		± 0.12	± 0.2	± 0.31
OZAB80‡	**Benthic 14C**		± 0.19	± 0.2	± 0.26
SST-3	**Tie point**		± 0.44	-	± 0.89
OZT822	**Planktic 14C**		± 0.16	± 0.2	± 0.28
OZAB81	**Benthic 14C**		± 0.16	± 0.2	± 0.29

Name	Type	Depth (cm)	^{14}C Yrs (ka BP, 1 error)	Reservoir Age (ka)	Mean Calibrated Age (ka cal BP, 95.4% C.I)
OZAB83	**Planktic 14C**		± 0.16	± 0.2	± 0.31
OZAB82‡	**Benthic 14C**		± 0.2	± 0.2	± 0.41
OZU083	**Planktic 14C**		± 0.14	± 0.2	± 0.3
OZAB84	**Benthic 14C**		± 0.22	± 0.2	± 0.3
SST-4	**Tie point**		± 0.35	-	± 0.4
OZAB86	**Planktic 14C**		± 0.19	± 0.2	± 0.29
OZAB85‡	**Benthic 14C**		± 0.26	± 0.2	± 0.5
OZAB88	**Planktic 14C**		± 0.22	± 0.2	± 0.27
OZAB87‡	**Benthic 14C**		± 0.36	± 0.2	± 0.21
OZT823	**Planktic 14C**		± 0.33	± 0.2	± 0.21
OZAB89	**Benthic 14C**		± 0.36	± 0.2	± 0.24
OZT824	**Planktic 14C**		± 0.4	± 0.2	± 0.34
SST-5	**Tie point**		± 0.37	-	± 0.43
SST-6	**Tie point**		± 0.49	-	± 0.5
SST-7	**Tie point**		± 0.51	-	± 0.53
SST-8	**Tie point**		± 1.18	-	± 1.12
SST-9	**Tie point**		± 0.96	-	± 1

Supplementary Figures

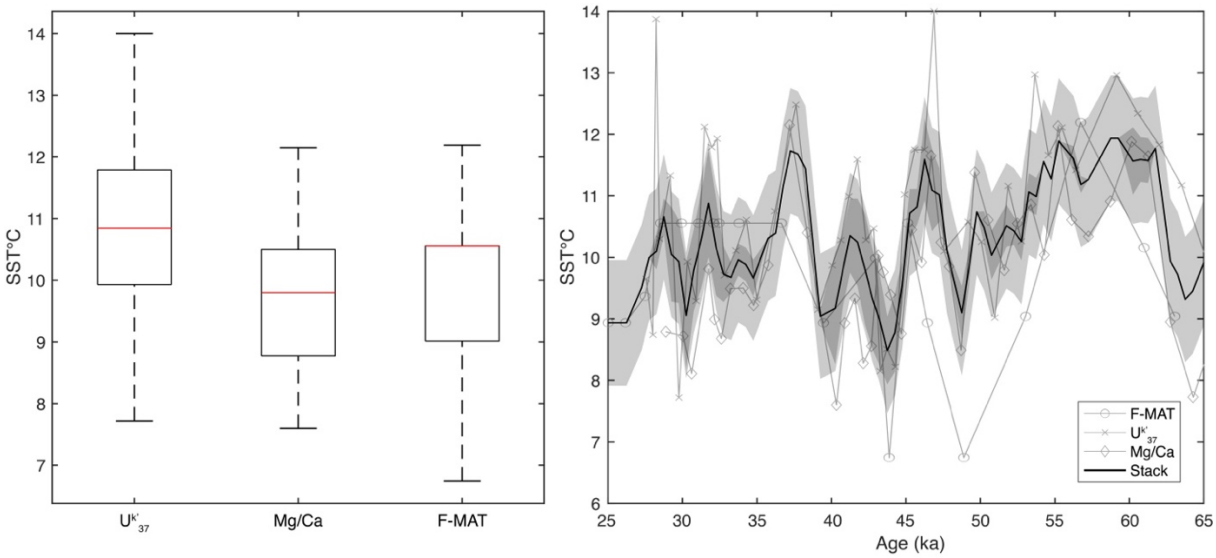

Figure S1. (Left) MIS-3 paleotemperature proxy distributions at TAN1106-28, where the red line represents the median temperature, the box is one standard deviation, and the dashed lines represent the range, and (Right) Paleotemperature proxies and multi-proxy mean binned to 500-year intervals. Light grey shading is the mean proxy error, dark grey shading represents the standard error in the mean.

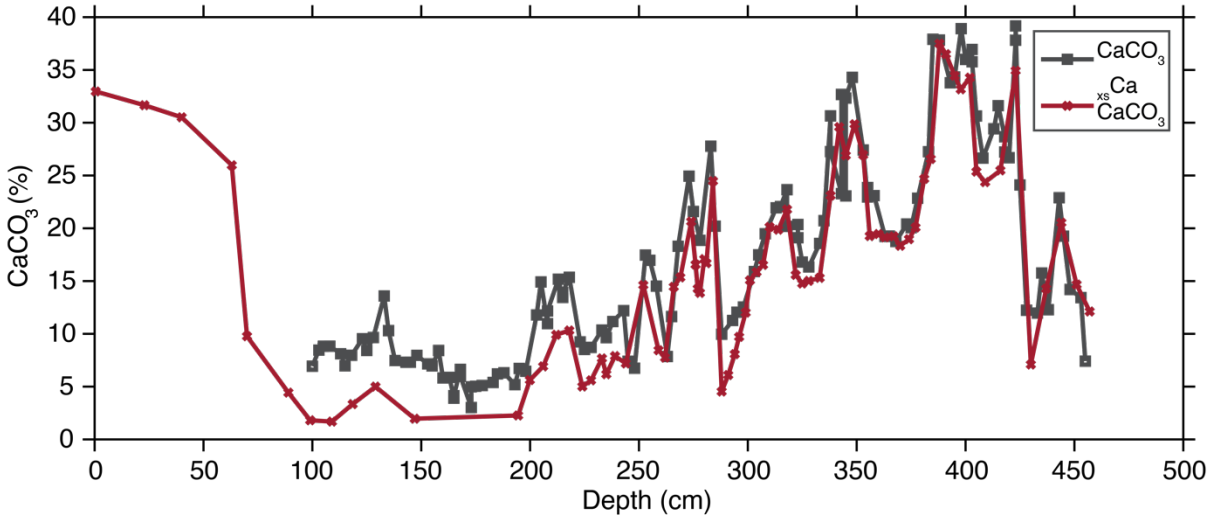

Figure S2. Depth plot of reconstrructed CaCO3 concentrations (black) and $_{xs}$Ca derived $CaCO_3$ concentrations (red). The similarity between the two measurements supports the use of the excess calculations for $CaCO_3$ and other proxies at TAN1106-28.

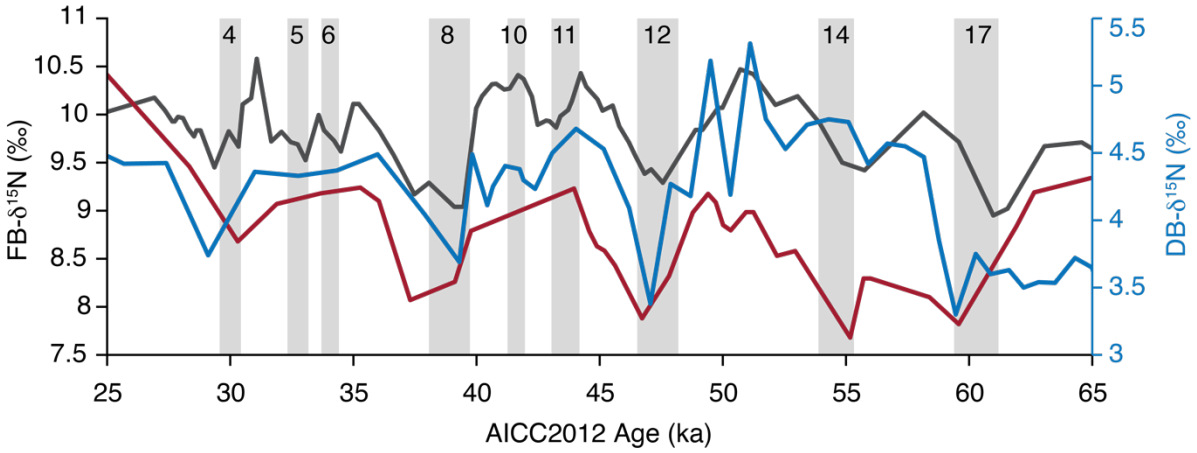

Figure S3. Comparison of subantarctic microfossil-bound ^{15}N records during MIS-3, with southwest Pacific TAN1106-28 (black), south Atlantic ODP-1090 (red; Martínez-García et al., 2014), and central south Pacific E11-2 (blue; Robinson et al., 2005). The E11-2 record is plotted on the right axis as diatom bound ^{15}N values are lower due to a reduced isotopic effect relative to foraminifera. Grey shading represents millennial-scale increases in Antarctic temperature (AIM events).